# Important Notice

THE UNIVERSITY OF CALGARY

# A MULTI-METHOD NEAR-SURFACE GEOPHYSICAL STUDY

# ON THE

# NOSE HILL UPLAND

by

Darryl G. Parry

A THESIS
SUBMITTED TO THE FACULTY OF GRADUATE STUDIES
IN PARTIAL FULFILMENT OF THE REQUIREMENTS FOR THE
DEGREE OF MASTER OF SCIENCE

DEPARTMENT OF GEOLOGY AND GEOPHYSICS

CALGARY, ALBERTA

DECEMBER, 1996

## Abstract

Five different geophysical techniques: ground penetrating radar (GPR), fixed frequency electromagnetics (EM), vertical electrical soundings (VES), seismic refraction and reverse vertical seismic profiling (RVSP) were applied during an investigation of the near-surface of the earth on the Nose Hill upland in northwest Calgary. These techniques tested radio, very low, and DC frequency electrical properties and elastic wave seismic properties of the shallow geological material at three survey sites.

The seismic velocity structure obtained via RVSP and refraction surveys revealed local stratigraphy and implied lithology. The addition of shear wave information identified probable climactic induced variations in water saturation. Refraction surveying was more successful in this locale than was RVSP, as logistical difficulties hampered the absolute location of seismic sources for the latter experiment.

The stratigraphic image produced seismically was supported by VES. The results produced by this electrical method suggested that GPR would be unsuccessful in areas with thick till cover. EM surveying allows an assessment of local electrical homogeneity and an areal extension of the VES interpretation. Where tills have been removed, GPR surveying was very effective and produced a clear, detailed picture of the braid plain gravels.

## Acknowledgements

# Table of Contents

# List of Tables

# List of Figures

## List of Symbols, Abbreviations, Nomenclature

**3-C** - three component. In this study, a seismic experiment in which the seismic waves are recorded in three orthogonal directions.

**6-C** - six component. In this study, a seismic experiment in which the seismic waves are recorded in three orthogonal directions and sources employed in two of these directions.

**AGC** - automatic gain control. A scheme for applying gain to a time series trace in which the gain is determined by the average absolute amplitude within a set gain window.

**Airwave arrival** - For GPR, the first arriving energy - passing directly from the transmitting to the receiving antenna.

**Apparent Resistivity** - A measurement in units of electrical resistivity which yields insight into the true resistivity of the earth. For VES, these measurements can be resolved to obtain true resistivity.

**Attenuation ($\alpha$)** - A measure of the tendency of a material to absorb the energy in a broadcast signal.

**Bandpass filter** - A filter which allows the passage of a restricted frequency component and attenuates others.

**CMP** - common midpoint. The central point of reflection for rays with different travel paths

**Common Receiver Gathers** - A seismic section constructed of traces recorded at a particular receiver.

**Critical Angle** - The angle of impingement of a seismic ray at which the ray first refracts at 90°.

**Critical Distance** - The source-receiver offset which will allow the first refracted arrival from a given interface.

**Dielectric constant ($\kappa$)** - A measure of the extent to which the electric charge distribution in a material can be polarised by the application of an electric field. Dielectric effects dominate conductive properties at high frequencies for most geological materials.

**Downgoing waves** - For a VSP, those seismic waves which are travelling downward when recorded. For an RVSP, those seismic waves which are travelling downward when they leave the source point.

**Electrical conductivity** ($\sigma$) - A measure of the ability of a material to pass electric current.

**EM** - electromagnetic(s). A group of geophysical techniques which depend on the measurement of a local electromagnetic field to infer the electrical nature of the earth.

**FEM** - fixed frequency electromagnetics. A type of EM surveying in which the instruments operate at a single frequency.

*f/k* **domain** - frequency/wavenumber domain. Time series data are often transformed into the *f/k* domain to effect separation of features whose velocity differ.

**First Arrivals** - Those seismic events which appear first on each trace of a record.

**First Breaks** - The first seismic energy to arrive on a record.

**Generalised Reciprocal Method (GRM)** - A seismic refraction interpretation method using source points at either end of a linear spread of seismic receivers. GRM assumes that arrivals from either source point leaving the refractor at nearly the same point may be recorded on different receivers. Analysis tools (Velocity Analysis Function and Time-Depth Function) attempt to identify these receiver pairs.

**GPR** - ground penetrating radar. An electromagnetic geophysical technique that consists of broadcasting a radar frequency wave into the earth and recording its refractions and reflections.

**Groundwave arrival** - For GPR, the second arriving energy. It is a guided wave, travelling along the surface of the earth at the velocity allowed by the most shallow materials.

**Median Filter** - A filter which operates by passing the median of a number of amplitude values from several traces.

**NMO** - normal moveout. The time difference between an assumed vertical reflection path and the travel path followed by a non-zero offset source/receiver pair.

**Ormsby filter** - A frequency filter. The Ormsby filter is defined by four frequencies: low cut, low pass, high pass and high cut. All amplitudes falling between low pass and high pass are unaffected. Amplitudes below low cut and above high cut are eliminated. Amplitudes falling between low cut and low pass and between high pass and high cut are reduced by a weighting factor.

**Phantoming** - A method for extending the refraction traveltime record into and beyond the crossover distance.

**Plus-Minus** - A seismic refraction interpretation method using source points at either end of a linear spread of seismic receivers. The plus-minus method assumes that seismic waves arriving from either source point at a single receiver refract upward at very nearly the same place.

**Radial component** - That component of received seismic signal which lies in the horizontal plane, in line with the source location.

**RET** - Reverse vertical seismic profile Extracted Trace. The stacked trace produced by processing a near offset common receiver gather in a RVSP survey. This allows correlation between geology in depth and a seismic section in two-way time.

**RRE** - radar range equation. An equation which attempts to account for all energy losses between transmission and reception of a radar signal. The RRE allows one to calculate the likely efficacy of radar surveying in a specific set of circumstances.

**RVSP** - reverse vertical seismic profile. An experiment in which seismic sources are expended in a wellbore and the resulting signal is recorded on the earth's surface.

**S/N** - Signal to noise ratio.

**Schlumberger array** - A specific arrangement of a current and potential dipole which allows for the recording of vertical electrical sounding data.

**SH mode** - Shear waves travelling with particle displacement in the horizontal plane.

**Slope/Intercept** - A seismic refraction interpretation method which assumes a multi-layered earth, all of whose layers are flat and horizontal.

**SSC** - signal saturation correction. An essential processing step in GPR interpretation. SSC removes the effect of a DC shift and slowly decaying wow on recorded traces.

**Static Shifts** - Refers to the amount of time adjustment necessary to reduce a seismic section to a single time datum.

**SV mode** - Shear waves travelling with particle displacement in the vertical plane.

**Time series** - A recording of signal amplitude versus time.

**Time-Depth Function** - An intermediate step in GRM interpretation. The time-depth function attempts to define the XY spacing. This is the distance between each pair of receivers which will record seismic arrivals leaving the refractor from nearly the same location, but coming from opposite directions.

**Transverse component** - That component of received seismic signal which lies in the horizontal plane and in a plane orthogonal to the radial component.

**Tube wave** - An interfacial wave which travels along the cylindrical fluid-solid boundary of a borehole at a low, relatively fixed velocity and exhibits no spherical divergence. Tube waves are one of the basic modes by which seismic energy propagates in VSPs and RVSPs.

**Upgoing waves** - For a VSP, those seismic waves which are travelling upward when recorded. For an RVSP, those seismic waves which are travelling upward when they leave the source point.

**Velocity Analysis Function** - An intermediate step in GRM interpretation. The velocity analysis function attempts to define the XY spacing. This is the distance between each pair of receivers which will record seismic arrivals leaving the refractor from nearly the same location, but coming from opposite directions. It also defines the velocity of each layer.

**Velocity Dispersion** - the variation of velocity with frequency.

**Vertical component** - That component of received seismic signal which lies in the vertical plane.

**VES** - vertical electrical sounding. A technique whereby electrical current is introduced to the earth and the resulting potentials are measured. This technique yields an understanding of the electrical layering of a multi-layered earth.

$V_P/V_S$ - Ratio of compressional wave velocity to shear wave velocity in a medium.

**VSP** - vertical seismic profile. An experiment in which seismic sources are expended on the surface and the resulting signal is recorded in a wellbore.

**Chapter 1. Introduction**

**1.1 Motivation**

This thesis deals with the application of several geophysical techniques to the investigation of the shallow earth. There are a variety of reasons for using geophysical techniques to investigate the shallow earth (the upper 100 or so metres), including mineral exploration, engineering design, archaeology and environmental studies. All of those methods which have been applied to deeper targets can be applied in the near-surface. Practically though, some techniques are more applicable to shallow investigations than are the rest. Logistical considerations favour certain techniques over others (refraction seismic surveying is simpler to conduct at very close offsets than conventional reflection seismic, for instance). The confidence in any geophysical investigation is improved by the investigation of a multiplicity of earth parameters (Dobecki and Romig, 1985). The experiments undertaken as part of this work include: seismic refraction, a shallow reverse vertical seismic profile (RVSP), vertical electrical sounding (VES), electromagnetic surveys (EM) and ground penetrating radar (GPR).

Shallow investigations may also be applied to clarify the image obtained by studies whose focus is deeper in the earth. Surface acquired geophysical measurements of the deeper earth are all affected to some degree by the filtering (or dilution) effect of the shallow earth. The effect of the near-surface varies with the type of geological material present in the shallow zone and with the investigative technique employed. It is useful to quantify these effects in order to mitigate their impact on deeper looking surveys. In particular, static shifts in seismic reflection surveying may derive from lateral variations in near-surface velocity (as well as variations in thickness of these layers). Static shifts are substantially greater in quantity for shear wave and converted shear wave studies than for compressional waves; shear wave velocity may be significantly lower in the near-surface than is compressional wave velocity (Wiest and Edelmann, 1984; Lawton, 1990). $V_P/V_S$ in the near-surface may be as great as 10 (Stümpel et al., 1984).

**1.2 Objectives**

The purpose of the work performed in this thesis is two-fold: firstly, to characterise the near-surface at the survey location and secondly, to identify among a multiplicity of geophysical techniques those methods which together provide a useful compendium for shallow earth investigations.  It is worthwhile to produce and provide measurements of physical parameters at a specific site; this adds to the body of information available to a person who is trying to generate realistic physical models of the earth.  It is also worthwhile to assemble a toolkit which can be readily applied to near-surface investigations.

**1.3 Data Suites**

The quintet of geophysical techniques discussed in this thesis were applied in the order: 1) RVSP, 2) refraction, 3) GPR, 4) EM, and 5) VES.  This abundance of methods was chosen to test the utility of multi-method studies.  The RVSP was a pure experiment to test data acquisition techniques and to observe the image  that could be obtained with them.  A refraction survey was conducted at the same time as the RVSP, but did not contain the information necessary to completely image the very shallow earth (there were no long-offset shots).  A second refraction survey was undertaken to rectify this and to provide more detail.  GPR was tested to identify whether electromagnetic physical parameters at radar frequencies would investigate different geological details than would acoustic physical parameters at seismic frequencies.  EM surveys provided a rapidly acquired data suite. This was interpreted to observe the variation in heterogeneity of earth conductivity within limited depth intervals over a broad area surrounding the RVSP site.  By inferring a correlation between lithology and conductivity, the observations gained using other methods could then be extended outward.  VES provides a useful companion piece to EM as it yields absolute (although not unequivocal), quantifiable estimates for the variation of electrical conductivity with depth.

The three-component (3-C) RVSP data set was acquired in August of 1993 by University staff and students during the annual geophysical Field School.  It consists of

twenty seven 32-station shot records. Two orthogonal lines of 16 receivers each were arrayed about the experiment wellbore. A suite of refraction data was recorded into these 32 receivers plus an additional 8 off-end the eastern line. The second refraction spread (a 6-C survey) consisted of a single line of forty 3-C receivers aligned east/west over the wellbore. This latter refraction survey was completed in June of 1994. GPR profiles were obtained in April and May of 1994 at the farm and gravel pit sites; common midpoint gathers (CMPs) were collected at each of the gravel pits. EM data were collected in June of 1994. These data were acquired at a dominant 20 metre by 20 metre spacing in a grid surrounding the wellbore. The final data collected were those for a single VES. This was performed at the wellbore location in July of 1995.

## 1.4 Survey Site(s)

The primary survey site lies in the northwest of the city of Calgary at the University of Calgary farm (sec. 28-25-2W5M - Figure 1.1). It is a relatively undisturbed, remote location with few nearby cultural features (excepting barbed wire fences) to interfere with geophysical measurements. Regionally, the farm is on an extended plateau (Nose Hill) with elevation of approximately 1,265 m asl. The local topography is generally flat.

All techniques discussed were undertaken at the farm site. EM and GPR was applied at the survey site itself and at two nearby gravel pits. The gravel pit operators remove the upper high electrical conductivity layer preparatory to mining aggregate. This allows for better penetration of the GPR signal than that which can be obtained in an undisturbed area. EM measurements in and immediately adjacent to the gravel pits suggest that the shallow earth is electrically similar in all three locations.
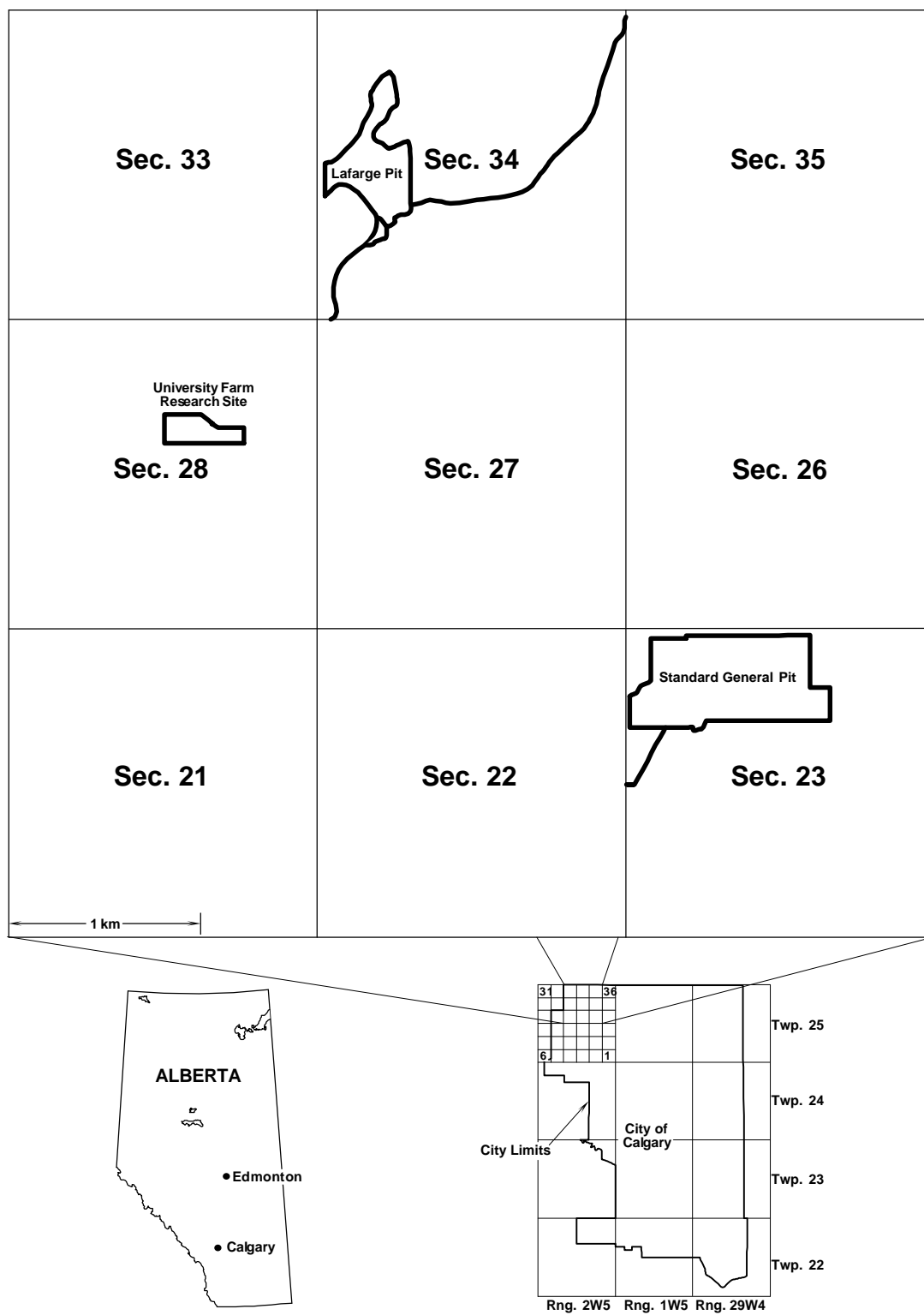
**Figure 1.1**  Location maps for survey site and nearby gravel pits tested via GPR and EM surveying.

## 1.5 Quaternary and Tertiary Geology of the Calgary Area

The uplands to the northwest and west of the city of Calgary are capped by up to 85 m of unconsolidated sediments (Moran, 1987). These materials can be broken into two broad units based on the dominant sedimentary processes involved; the upper unit (Lochend and Spy Hill Formations) is comprised of glacial till and the lower (Quaternary Gravels) of braid plain sand and gravel deposits (Osborn et al., 1991). The underlying bedrock is the Palaeocene Porcupine Hills formation.

At the survey site, the outcrop is of Lochend Formation tills. The Lochend is underlain by tills of the Spy Hill Formation which rest directly on Pleistocene gravels. The Lochend tills and the upper unit of the Spy Hill till are derived from Laurentide ice sheets, while the lower Spy Hill till has its source in the Cordillera (Moran, 1987). A generalised local stratigraphic column is shown in Figure 1.2.

The gravels are of economic interest locally where they have been mined for construction material. They can contain abundant amounts of carbonate material as cement. This causes concern to the operators of the gravel pits as the highly cemented gravels are of no use as aggregate and can cause severe difficulty in production of surrounding material.
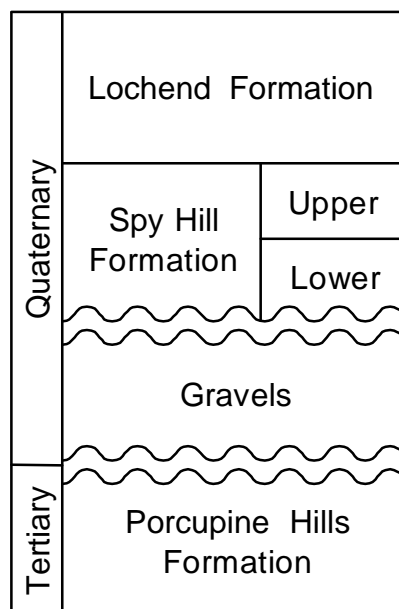
**Figure 1.2** Generalised stratigraphic column of the near-surface geology in the study area.

**Chapter 2.   RVSP**

## 2.1   Introduction

Reverse vertical seismic profiles (RVSP's) provide an opportunity to investigate the earth's composition and structure in fine detail (Jones, 1991; Hu, 1991).  When combined with three-component recording, an RVSP provide information regarding the propagation of shear waves as well as compressional waves.

Seismic methods in which the sources or receivers are placed in a wellbore provide some advantages over conventional surface recorded seismic surveys.  As a seismic wave passes through the earth, its character changes due to attenuation of high frequencies, velocity dispersion and absorption.  If the wave is sourced or measured within the earth (instead of on the earth), its total travel path length is less than it would be for a conventional survey so these effects are reduced (Cassell, 1984).  Additionally, VSPs and RVSPs allow a direct correlation between reflection events and geology, so that they may be used to study the reflection character of a zone in detail, and provide a ready means of observing variations in acoustic parameters such as $V_P/V_S$ (Balch et al., 1982).

In a RVSP (Figure 2.1) a number of sources are placed in a borehole and receivers are laid out on the ground surface.  These experiments may record arrivals at several surface locations simultaneously, limited only by the number of recording channels available.  It is also possible to easily determine the orientation of the receivers for a RVSP survey (an important consideration in multi-component recording).  It is not possible to easily determine the orientation of receivers for a VSP.  A *t-z* plot of RVSP arrivals (Figure 2.2) contains a number of linear features.  These features depend on the local velocity structure of the earth. Reflections all contain a downgoing path, direct arrivals are upgoing, and multiples may travel either path.
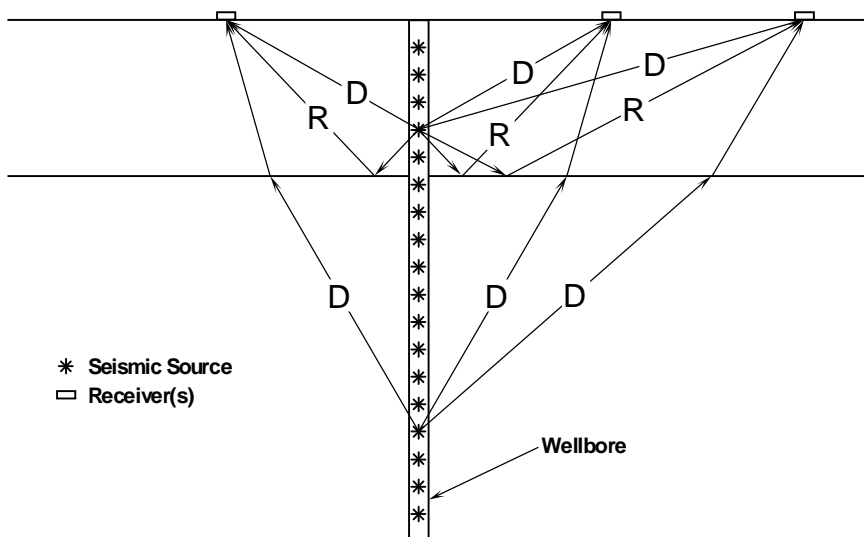
**Figure 2.1** RVSP raypath geometry.  D - direct arrivals, R - reflected arrivals.
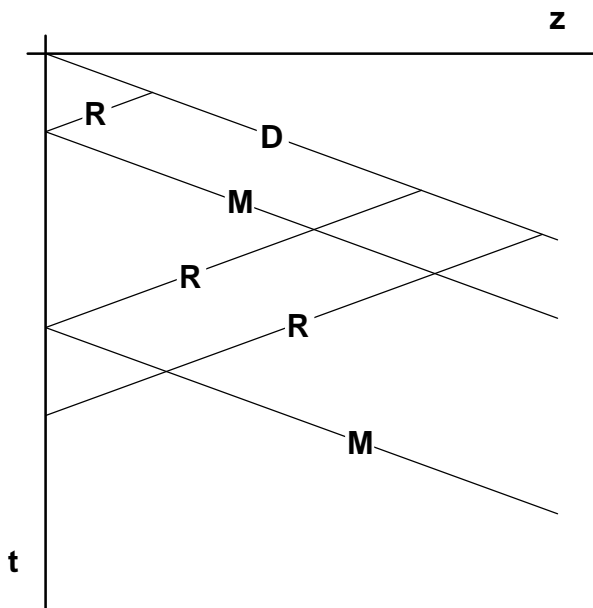
**Figure 2.2** Depth-time plot of RVSP arrivals for a receiver at zero offset from the borehole.  D - direct arrivals, R - reflections, M - multiples.

The primary concern for a RVSP is a suitable seismic source. It is difficult to implement a source which is capable of providing enough energy over significant distances to record useful seismic information and which will not damage the borehole. This is more of a concern in oil and gas exploration RVSPs where wells are deeper and more costly and which may be required to serve a purpose after the seismic survey is complete.

Multi-component RVSP's provide their own concerns. Critical to such a study is a determination of the nature of the shear wave source. Shear waves may be generated at the shot, may be converted from *P* at the borehole wall, or may be converted from tube-waves at the top of the fluid column. Additionally, shear waves are converted from *P*-waves striking acoustic impedance boundaries at non-normal incidence.

## 2.2  Data Acquisition

A shallow RVSP was acquired in August of 1993 during the University of Calgary Geophysics Field School. Three-component geophones were laid out in two orthogonal lines: one running north-south and one east-west. Both were centred on a 30 m deep borehole (Figure 2.3) which penetrated glacial tills and gravel deposits, but did not reach bedrock. Eight three-component OYO geophones were used on each of the four limbs radiating from the borehole. The near offset from the borehole to receiver was 2 m for each limb, with the remaining receivers placed at 2 m intervals. All receivers were planted with one component oriented vertically, one east/west, and one north/south.. Horizontal components in-line with their limb are referred to as radial, whereas those orthogonal to their limb are termed transverse. Shots were suspended on a shot cable in the borehole at one metre intervals from 1 to 30 m depth. The source employed was a 50 gm booster loaded in a cylindrical shell which was oriented vertically.

Each shot produced a 32 trace record for each of the three components. For these records, trace 1 is the most northerly receiver, trace 16 the southernmost, trace 17 is westernmost, and trace 32 the furthest east. Data were recorded to 1 second using a 2 ms sample interval. No data were acquired at depths of 4, 12, and 29 m due to shot misfires.
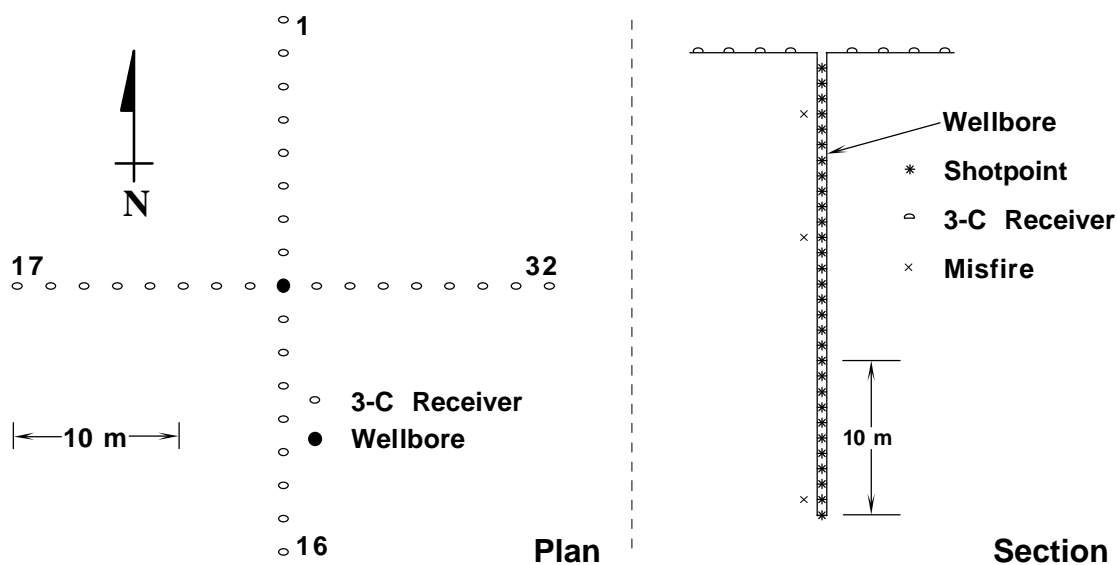
**Figure 2.3** RVSP survey geometry.

Once the original string of shots had been fired, an extra charge was prepared and fired at 5 m depth. The record thus acquired is a very close match to the original 5m deep record, except that it appears to contain less high frequency data.

## 2.3 Data Processing

### 2.3.1 Traveltime Inversion

Minimal processing was required for this portion of the analysis as it is concerned primarily with the direct arriving energy. IT&A's Insight software was used to pick the direct arrival times and to apply a 125 ms AGC and a 5/10-120/180 Hz bandpass filter to the plotted records. The records were also sifted to produce common receiver gathers in order to apply a forward vertical seismic profile (VSP) processing scheme.

### 2.3.2 RVSP Extracted Trace

VSP studies reference the wavefield to the receiver location. This makes sense as there is a simple distinction between the direct arriving (downgoing) and reflected (upgoing) wavefield at the receiver. That is not the case for RVSP, in which the

wavefield is entirely upgoing at the receiver. Reference is therefore made to the shot for RVSP surveys. The direct arriving wavefield is upgoing and reflection energy is downgoing at the shot (seismic waves that travel a multi-reflection path may be either upgoing or downgoing at the shot). Once this distinction is made, RVSP data can be processed in the same fashion as VSP data. RVSP common receiver gathers represent the same seismic events as would a VSP recorded with the shot located at the receiver location and geophones at the source locations. The raypaths travelled should be the same, but reversed (Chen et al., 1990).

The processing flow used for a near-offset RVSP is shown in Table 2.1. Gathering, geometry and first break picking are essentially pre-processing steps. Gathering to common receiver domain provides the VSP approximation. First breaks and geometry are required for velocity determination and wavefield separation.

**Table 2.1**   Near-offset RVSP Processing Flow

| |
|---|
| Gather to Common Receiver |
| Geometry |
| Pick First Breaks |
| Wavefield Separation |
| Deconvolution Design Upgoing |
| Deconvolve Downgoing |
| Corridor Stack |

Wavefield separation is accomplished by filtering out events that are nearly parallel to the first breaks. This is most commonly done by aligning the traces on first breaks, applying a median filter to the gather and subtracting the filtered output from the input gather (Kommedal and Tjøstheim, 1989). Another technique is to transform the data to the *f/k* domain and effect wavefield separation there (Chen et al., 1990). The upgoing and downgoing waves should map into different areas in the *f/k* domain as they exhibit opposite dips in time.

The direct arrivals are used to design a deconvolution operator for the downgoing data set as they are assumed to approximate the wavelet closely. The deconvolution operator is applied to the downgoing wavefield which is then bandpass filtered to improve S/N. Finally, the traces are muted to remove direct arrivals and late time arrivals which are dominated by noise and are stacked to produce the RVSP extracted trace (RET).

Figures 2.4 and 2.5 are gathers for the receiver 2 m west of the borehole (vertical and radial component respectively[2.1] ). The first arrivals of shear wave energy (i.e. earliest arriving high amplitude events) on the radial component are partially obscured by earlier arriving compressional waves. The impulsive source used in this experiment suggests that the wavelet should be minimum phase, but the direct arrivals appear distinctly zero phase, probably a result of instrument response.

Several attempts at deconvolution were made for these data, none of which showed substantial improvement in data quality. Zero phase deconvolution was one of the attempted methods, suggested by the zero phase appearance of the direct arrivals. The fully processed results reported here have not had any deconvolution applied to the data.

Wavefield separation was attempted via both *f/k* filtering and median filtering the aligned upgoing wavefield. In both cases the downgoing information was degraded in the process. Given the geometry used in this experiment, especially its extreme shallowness, the upgoing and the downgoing wavefields exhibit little difference in trace to trace moveout, so that any technique depending on velocity variation in the two wavefields will not separate them effectively. The decision was made to proceed with the stack without explicit wavefield separation. The upgoing wavefield should contribute less to the final gather as its stronger events are relatively early and partially muted. The stacking process should also reduce its effect.

---

[2.1] Transverse component data contains much the same information as does the radial component, but is degraded in S/N.
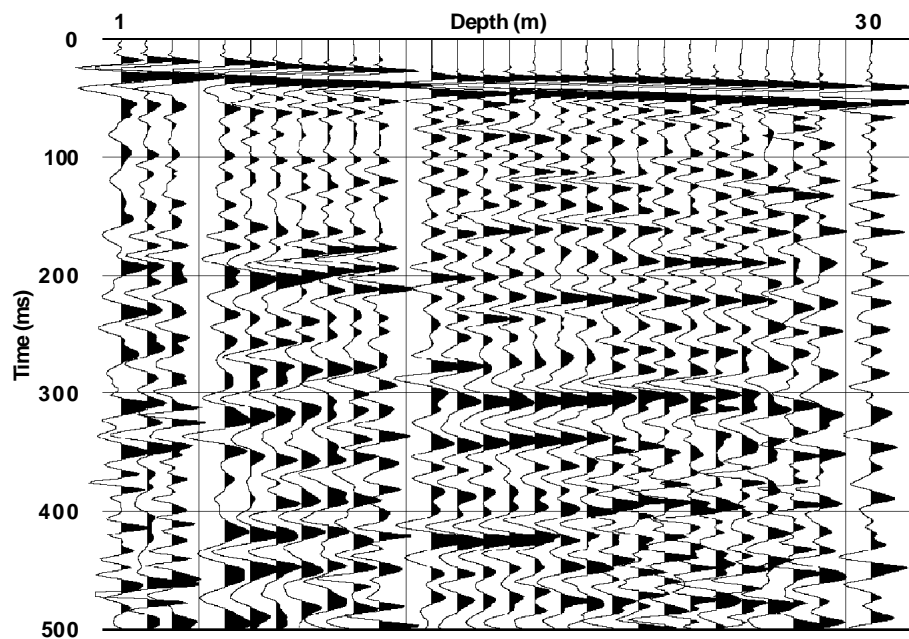
**Figure 2.4** Vertical component common receiver gather - 2m west offset receiver.
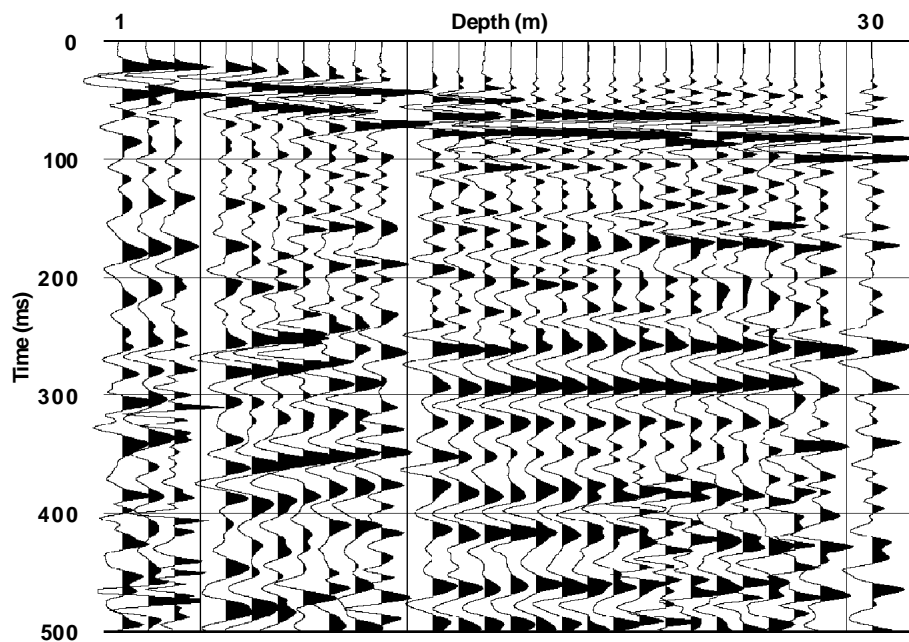


**Figure 2.5** Radial component common receiver gather - 2m west offset receiver.

## 2.4  Interpretation

### 2.4.1  Traveltime Inversion

Figure 2.6 is a shot gather for shot 27.  Figures 2.7 and 2.8 are plots of the early time (first 200 ms) for shot 27 and 16 respectively.  The shot numbers equate to depth in metres.  Direct arriving *P*-waves are well-defined and clear on the vertical component records.  The horizontal components present more difficulty in interpretation.

Radially oriented components record first arrivals that are reasonably easy to identify.  The shear wave first arrivals are not, however, the first signals recorded on the transverse component.  They are somewhat obscured by *P*-wave energy leaking onto the horizontal components.  This is especially true for the shallow shots at near offsets, making first arrival picking difficult (and sometimes impossible).  The apparent polarity of these radial traces flips by 180º across the borehole.  This is most clear for the direct arrivals on Figures 2.7 b), 2.7 c), 2.8 b) and 2.8 c).

Transverse components record even lower signal to noise ratios (S/N) than do the radial components.  This possibly results from the cylindrical shape of the source and borehole - less transverse oriented shear is generated than is radial shear.  An examination of all records suggests that the deeper shots provide the lowest S/N for transverse components, with an improvement for shots further uphole.  The polarity of first arriving shear on the transverse component is less predictable than that for the radial component. No analysis of the transverse direct arrivals has been performed as the quality of picks is too poor.
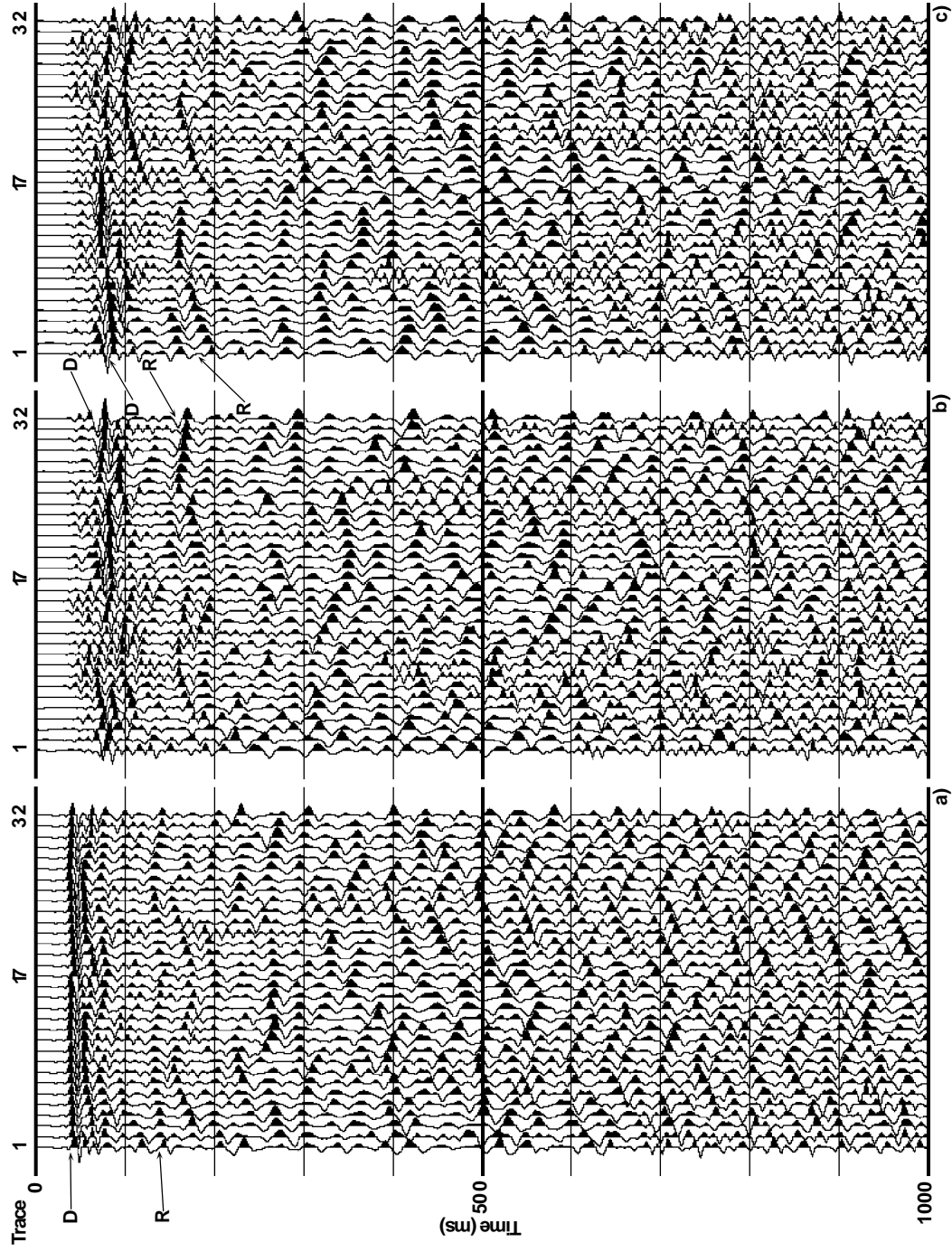
**Figure 2.6** Shot gathers for a) vertical, b) east-west, and c) north-south oriented components. Shot at 27 metres depth. Traces 17-32 of b) and 1-16 of c) are radial. Direct arrivals- D, reflections - R.
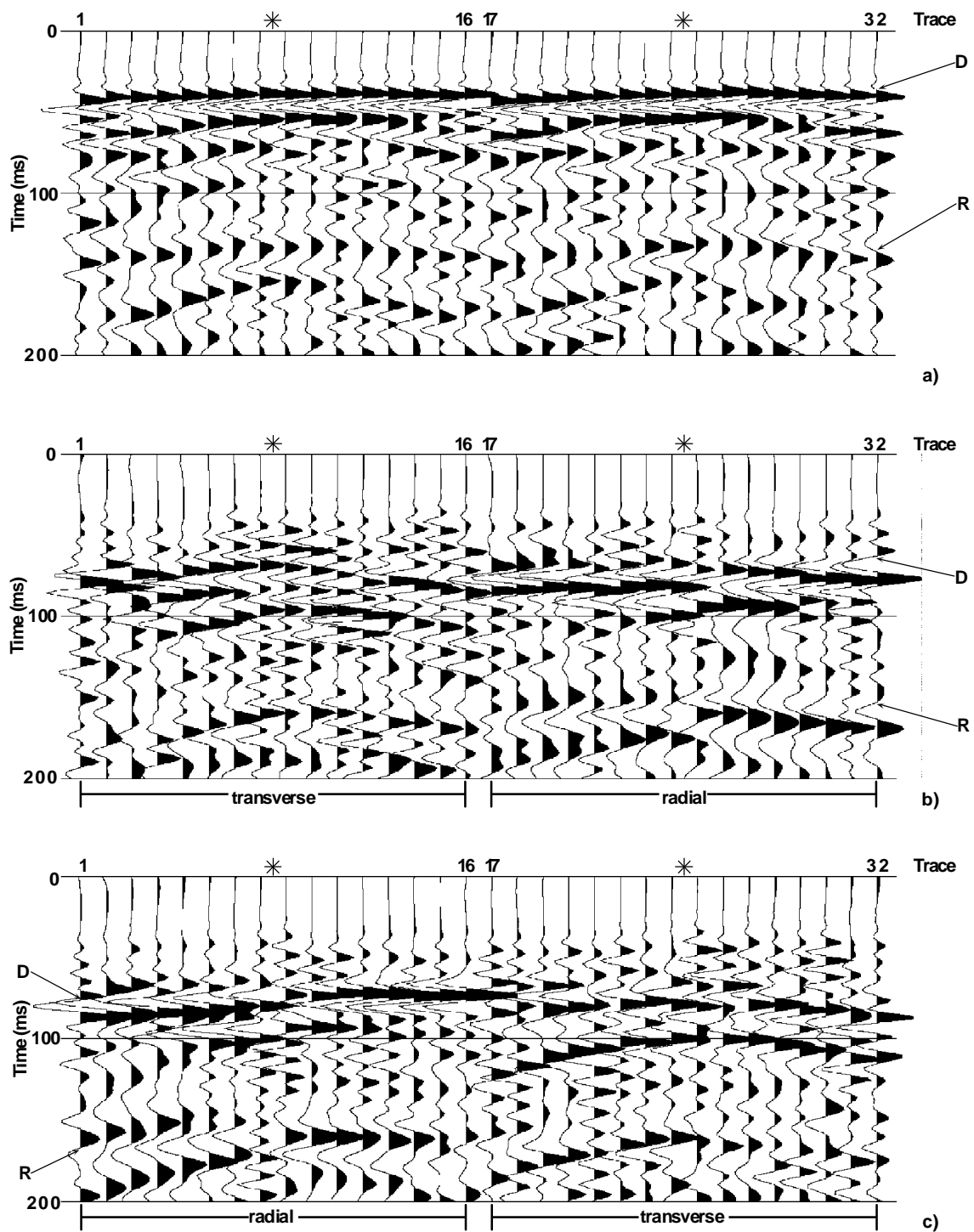
**Figure 2.7** Shot gathers for a) vertical, b) east-west, and c) north-south oriented components. Asterisks show shot position. Shot at 27 m depth. Traces 17-32 of b) and 1-16 of c) are radial. Direct arrivals - D, reflections - R.
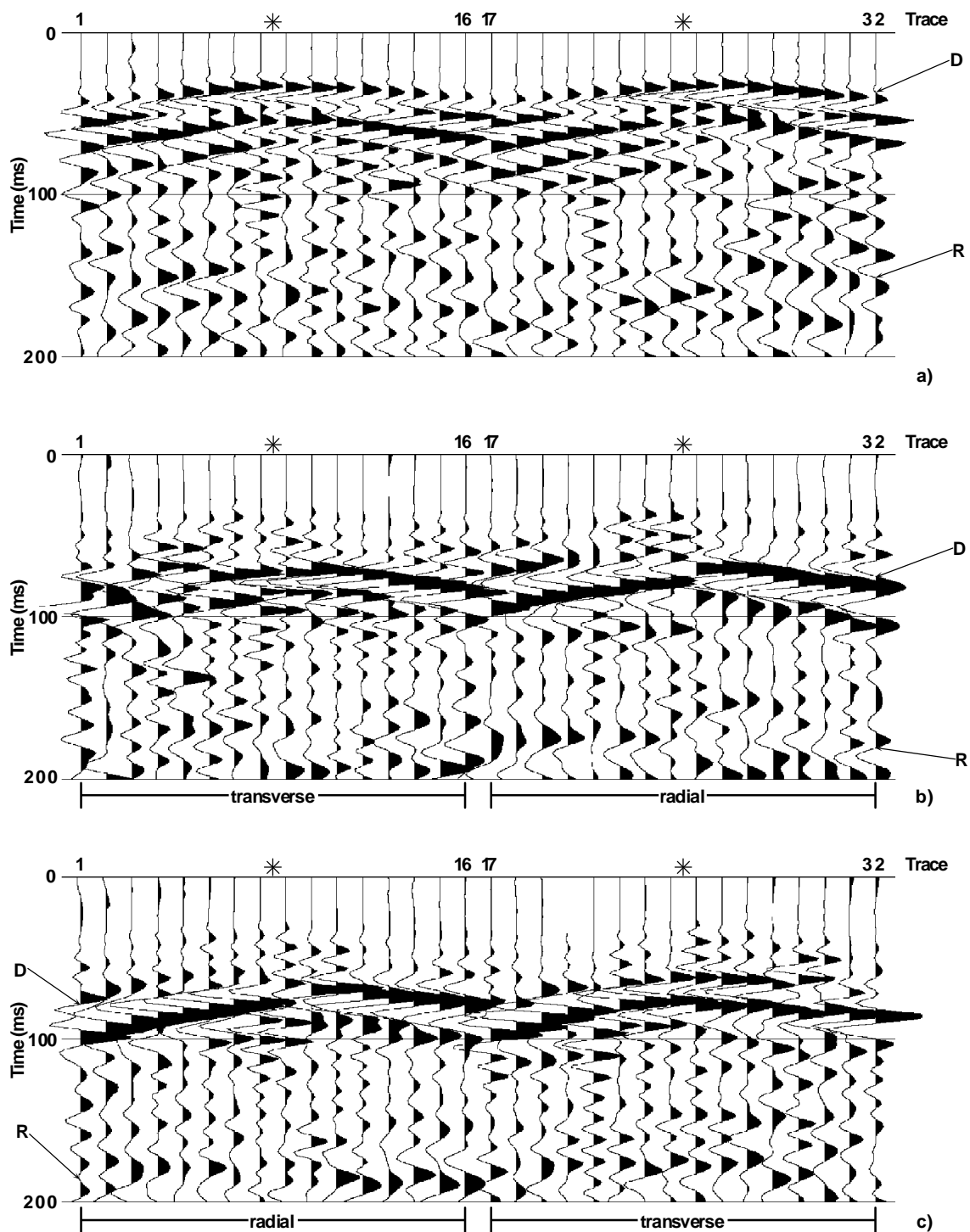
**Figure 2.8** Shot gathers for a) vertical, b) east-west, and c) north-south oriented components. Asterisks show shot position. Shot at 16 m depth. Traces 17-32 of b) and 1-16 of c) are radial. Direct arrivals - D, reflections - R.

A *t-z* velocity analysis has been performed for each of the near offset (2 m) receivers (Figure 2.9). This was performed by plotting shot depth versus direct arrival time. In much the same manner as a refraction survey, velocity is determined as the inverse of the slope of such a graph. This analysis only applies, strictly speaking, to a zero offset receiver. Compensation for offset was performed by assuming a straight raypath and reducing recorded traveltime values by the factor cos $\alpha$, where $\alpha$ is the angle between the borehole and a straight line drawn from shot to receiver. There is little appreciable time compensation for shot depths greater than 5 m at 2 m offset. The traveltimes shown in Figure 2.9 have had this compensation factor applied.
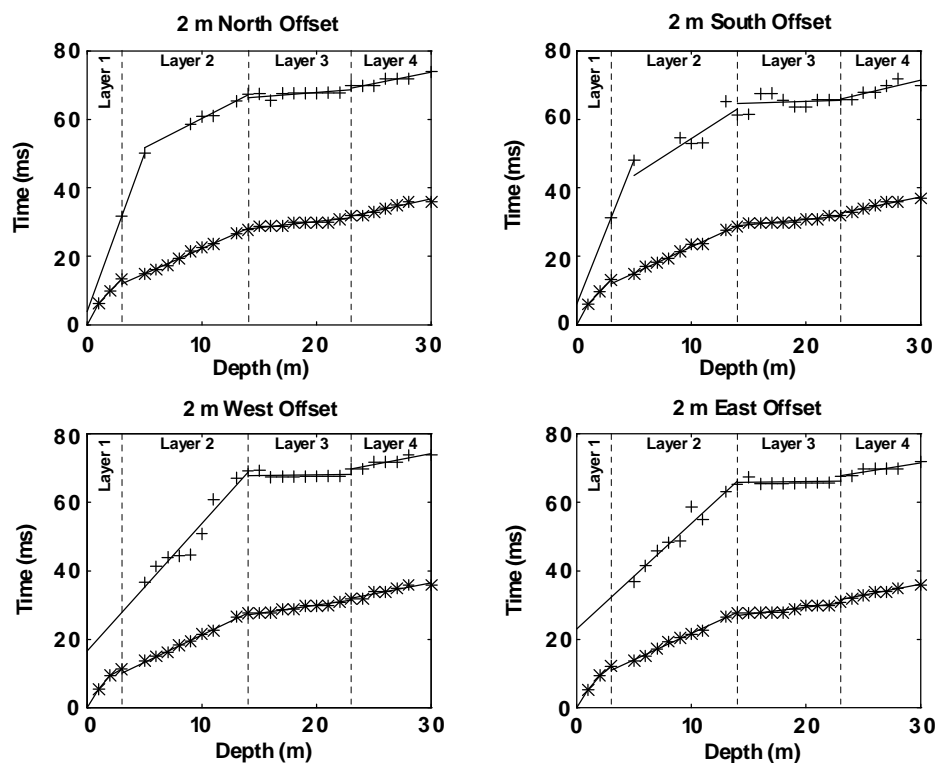
**Figure 2.9** Time/depth curves for the near offset (2 metre) receivers. + = radial component, * = vertical component.

The velocities thus derived are presented in Table 2.2. Errors are obtained as standard error of the estimate, and reflect the scatter in traveltimes. There are some residual directional effects (perhaps deriving from wellbore deviation) that result in the

relatively large variations in velocity.  The compressional wave velocities ($V_P$) behave as expected for layers 1, 2, and 4.  Layer 3 shows substantially higher velocity than surrounding layers, but the scatter in values is much greater.  The shear wave velocities (radial component) are interpretable for layer 2 only.  The slopes of the radial arrivals for layers 3 and 4 match closely those for the vertical component.  This suggests that the direct arrivals from the deeper shots at the near offset travel as compressional waves below 14 m depth and are only then converted to *S*-waves.  No shear wave velocity was obtainable, therefore, for layers 3 and 4.  Layer 1 *P*-wave arrivals have particle motion contained primarily in the horizontal plane.  This, coupled with the smaller difference between *P*- and *S*-wave traveltimes in the shallow earth made interpretation of Layer 1 shear wave velocities impossible.

**Table 2.2**   Interval velocities from *t-z* analysis (m/s).

| Layer | | North | South | West | East | Average | Error |
|---|---|---|---|---|---|---|---|
| 1 | Vertical | 280 | 280 | 340 | 290 | 300 | ±25 |
| 2 | Vertical | 680 | 650 | 630 | 650 | 650 | ±20 |
| | Radial | 350 | 400 | 270 | 320 | 340 | ±35 |
| 3 | Vertical | 2860 | 3310 | 2060 | 2390 | 2660 | ±330 |
| 4 | Vertical | 1390 | 1510 | 1540 | 1540 | 1500 | ±200 |

The interval depth boundaries are defined by the points at which the *t-z* slope changes.  At the wellbore, layer 1 is 3 m thick, layer 2 is 11 m, layer 3 is 9 m, and layer 4 at least 7 m thick.  The velocity structure and local outcrop suggests a stratigraphic correlation of layer 1 to till, layer 2 to saturated till, layer 3 to cemented gravels and layer 4 to uncemented gravels.  An alternative interpretation is possible.  The explosive sources used for this experiment were suspended by cable in a mud-filled borehole.  It was not possible to monitor the exact spatial location of the sources during the study and the explosions at lower depths may have affected the elevation of the shallower sources before they were used.  Other geophysical data (which will be discussed later) do not

disallow that the apparent third layer results from the displacement of sources between about 14 and 23 metres depth.

One of the potential difficulties in this type of survey is characterisation of the shear wave source. It is possible that *S*-wave energy is being converted from tube-wave energy at the top of the fluid column. If this is the case, the *S*-wave moveout will be uniform for all records obtained from shots below the top of this column. This was tested by determining stacking velocities for the *S*-wave event for all shots after bulk shifting each record so that $t_0$ was equal for each shot depth. These stacking velocities (Figure 2.10) increase with shot depth, suggesting that *P*-wave to *S*-wave conversion is not occurring at a single depth level. The *t-z* velocity analysis, however, suggests that the near offset receivers record shear wave energy generated from compressional waves from sources below 14 m depth. It is, at first, surprising that the vertical and horizontal components produce similar stacking velocities, but deeper *S*-wave arrivals travel most of their path as *P*-waves.

## 2.4.2  RVSP Traveltime Modelling

The geometry of the RVSP survey is such that many of the seismic events which represent boundaries within the wellbore depth interval follow raypaths with reflection angles greater than the critical angle. This suggests that the first arriving energy at varying offset (and especially at far offset) may not be direct arrival energy, but may travel by some more complicated path. This has implications for RVSP processing. In an effort to better understand the early arriving energy in the field data, a simple velocity structure and the RVSP geometry were used as the basis for traveltime modelling.

Nine possible events are considered (Figure 2.11). For sources in the uppermost velocity zone ($V_1$); direct arrivals, reflections, and critically refracted arrivals from both impedance boundaries are computed. In the second zone ($V_2$); direct arrivals, reflections and critical refractions from the layer 2/layer 3 boundary are computed. Sources in the lowermost zone ($V_3$) provide direct arrivals only.
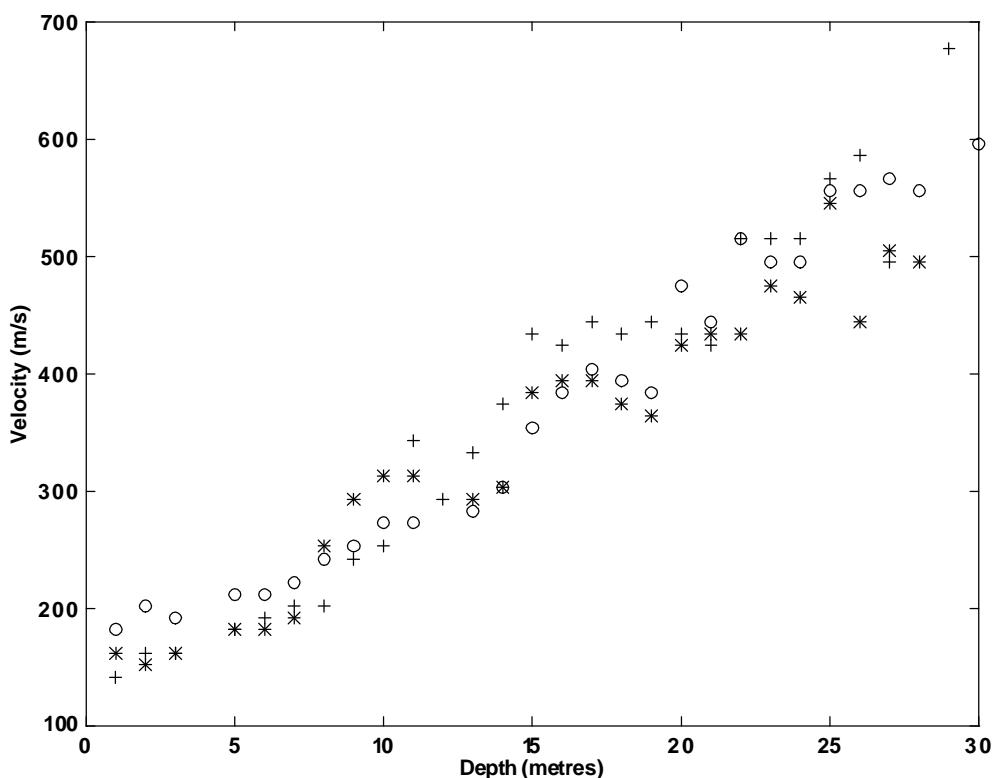
**Figure 2.10** Stacking velocities for radial records. NMO in the direct arrivals will be compensated for by these velocities. o = vertical component, + = east-west component, * = north-south component.

The program used to perform this modelling uses a series of equations depending only on geometry and Snell's law. Traveltime solutions were determined, and amplitude and phase of events were not considered. These equations are readily derivable, but several of them require an iterative solution. This approach was chosen as it is more easily implemented than a ray-tracing scheme. Results are presented in common receiver form. Figure 2.12 shows modelled arrival time graphs for both *P*- and *S*-wave events for the offset extremes of 2 and 16 m. The first arriving energy follows a direct arrival path for all depths for the near offsets, but is alternatively direct arriving or head wave arriving energy for the far offsets. The near offset cases show no post-critical arrivals. For the farthest offset receiver, post-critical reflections and critical refraction events occur for all sources (*P* and *S*) originating in the uppermost two layers. Post-critical events increase in

number with increasing offset until all but direct arrivals are post-critical beyond 8 m for compressional waves and beyond 6 m for shear waves.
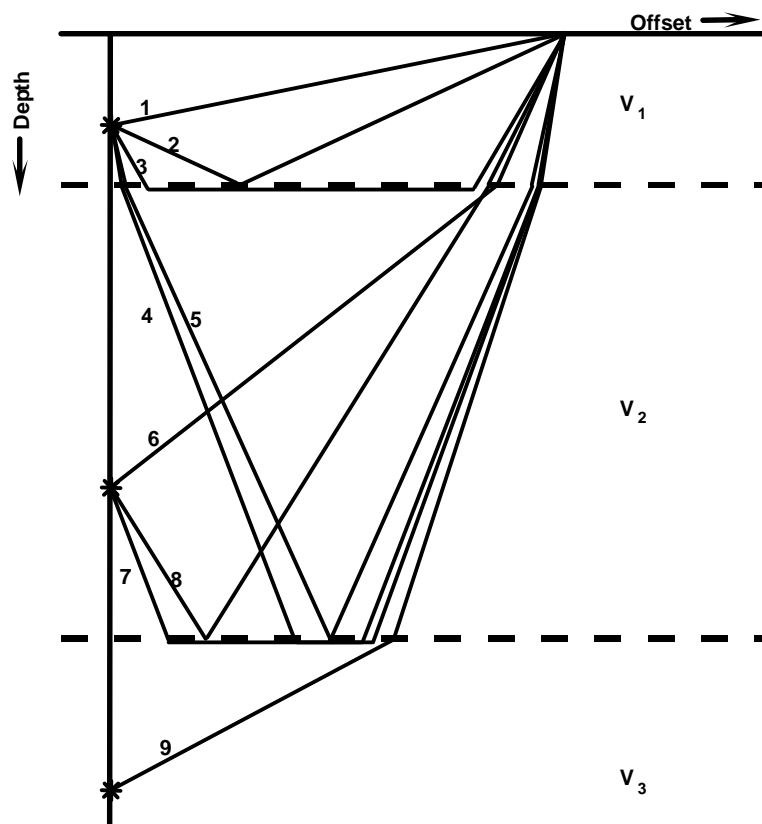


**Figure 2.11**   Raypaths for seismic events considered in modelling.  For sources in the first layer; 1) direct arrival, 2) ray reflected at first interface, 3) ray critically refracted at first interface, 4) ray critically refracted at second interface, 5) ray reflected at second interface.  For sources in the second layer; 6) direct arrival, 7) ray critically refracted at second interface, 8) ray reflected at second interface. Sources in the third layer contribute 9) direct arrivals.

The modelling suggests that the near offset common receiver gathers can be treated as a normal VSP data suite with appropriate consideration given to the sense of direction of the seismic wavefields involved.  The direct arrivals are not substantially obscured by other early arriving seismic energy (Figures 2.13 and 2.14).  This approach has been applied to both the vertical and radial component common receiver gathers for 2 metres offset.   The  modelled  traveltimes  indicated  on  the  figures  confirm  the

interpretation of direct wave arrivals for both the radial and vertical components. It is clear in Figure 2.14 that some energy (*P*-wave energy) arrives on the radial component receivers before the *S*-wave. The first strong event on this figure at depths below 13 metres are *S*-wave direct arrivals. Reflection events are not evident for either case as the gain applied to these images is quite low.

This traveltime modelling for the well interval arrivals suggests that a zero-offset VSP approach is suitable for processing the near offset receiver gathers from the RVSP survey. Post-critical reflections and head wave arrivals are observed at receivers offset more than 8 m in the *P*-wave case and 6 m in the *S*-wave case.
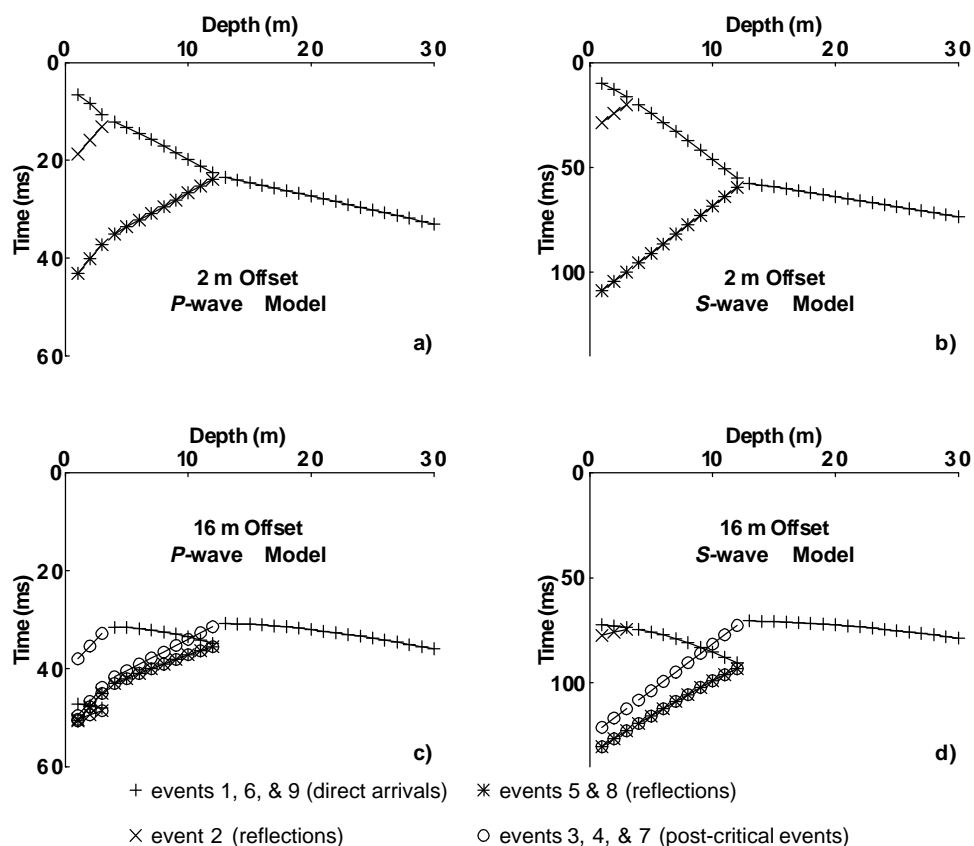


**Figure 2.12** RVSP traveltime models for the refraction velocity structure. a) is for a 2m offset *P*-wave receiver, b) is for a 2m offset *S*-wave receiver, c) is for a 16 m offset *P*-wave receiver, and d) is for a 16 m offset *S*-wave receiver.
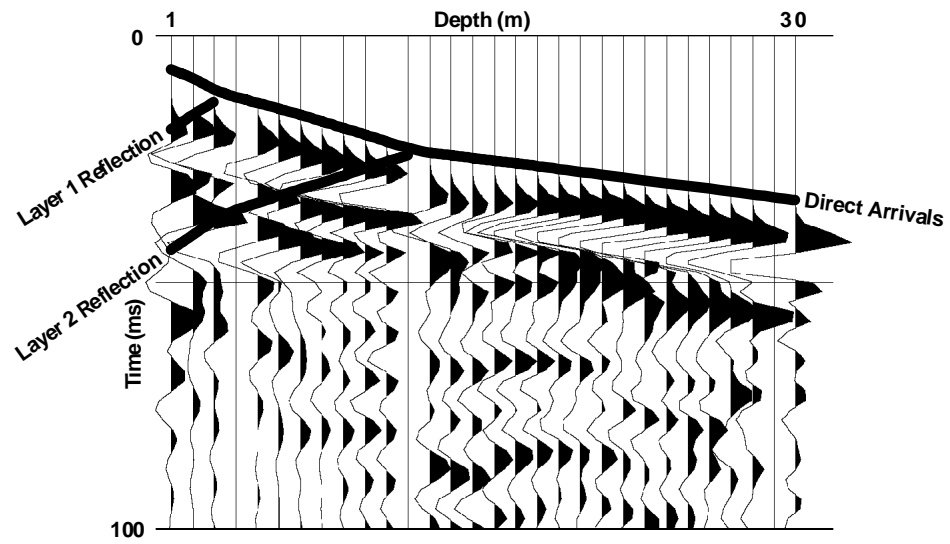
**Figure 2.13**    Modelled *P*-wave traveltimes overlain on early record section.  Vertical component data for 2m north offset receiver.
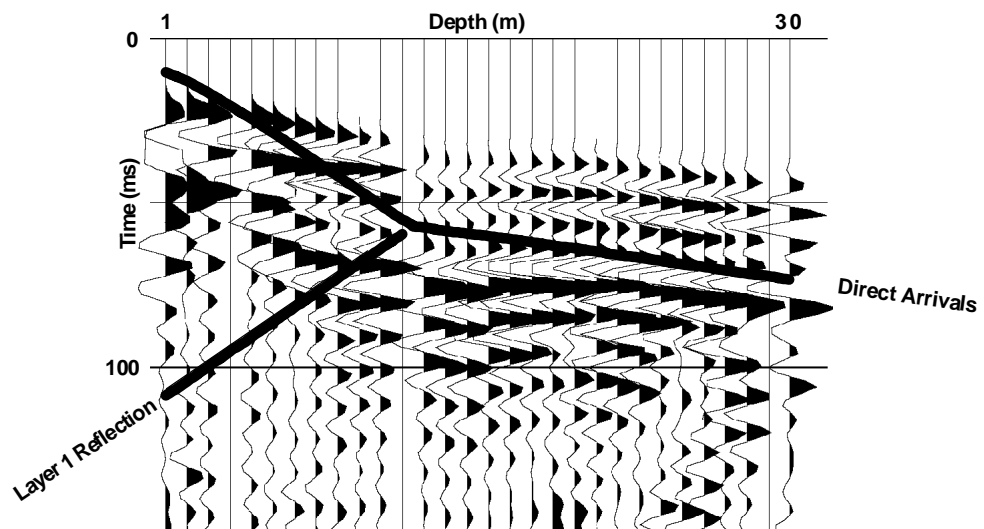


**Figure 2.14**    Modelled *S*-wave traveltimes overlain on early record section.  Radial component data for 2m north offset receiver.

### 2.4.3   RVSP Extracted Trace

Final RVSP extracted traces (RET's) and the aligned gathers from which they are derived are shown in Figures 2.15 and 2.16.  These were obtained from the 2 m west offset receiver.  On the vertical data, a strong trough doublet manifests itself at 300-375 ms, as does a strong peak at about 200 ms.  The trough/peak/trough triplet at about 130 to 150 ms is also evident on all near offset stacks.  Correlation of the other events in the zone 120-400 ms is less striking, probably resulting from the brute stack approach to the RET generation.  The radial component data exhibit greater correlatability, perhaps because the slower travelling shear waves are more completely separated during processing.  Events from about 220 ms to 480 ms on these stacks are all well correlated.

The reflection at about 190 ms time on the vertical component section comes from below the top of the Porcupine Hills Fm.  Its equivalent on the radial component RET should appear at about 255 ms traveltime (and is likely the prominent peak at about 240 ms).  The minimum two-way $P$-wave traveltime to the top of the Porcupine Hills is about 85 ms - or about 130 ms for the combined $P$- and $S$-wave travel paths assumed for the radial component RET.  The top of the Porcupine Hills is probably partly muted on both sections.  No openhole log information over this interval is available in the local area to assist in confirming or denying these interpretations.  Later arriving events are left unidentified because of the dearth of information which would allow a geological correlation.

Very shallow RVSP surveys do not allow the full VSP processing approach to be implemented completely.  Wavefield separation is particularly problematic as upgoing and downgoing waves differ little in trace to trace moveout.  However, a brute stack approach with no wavefield separation beyond stacking shifted traces has been shown here to provide interpretable RETs.
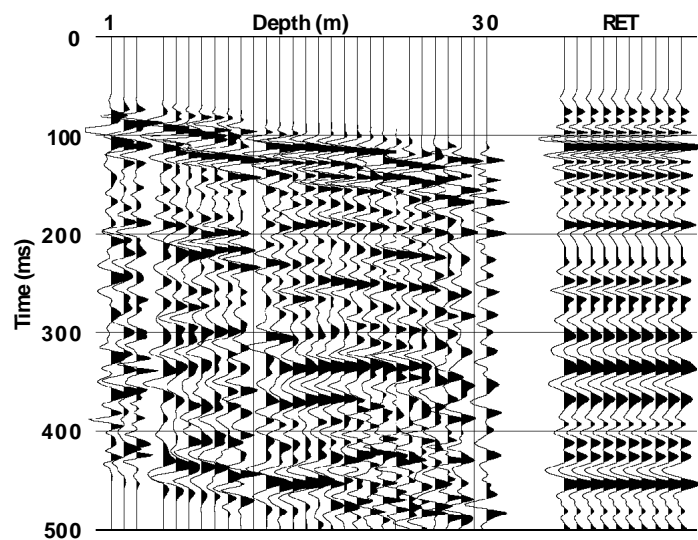
**Figure 2.15**   Aligned downgoing wavefield and RET.  Vertical component (i.e. *P*-wave) data.
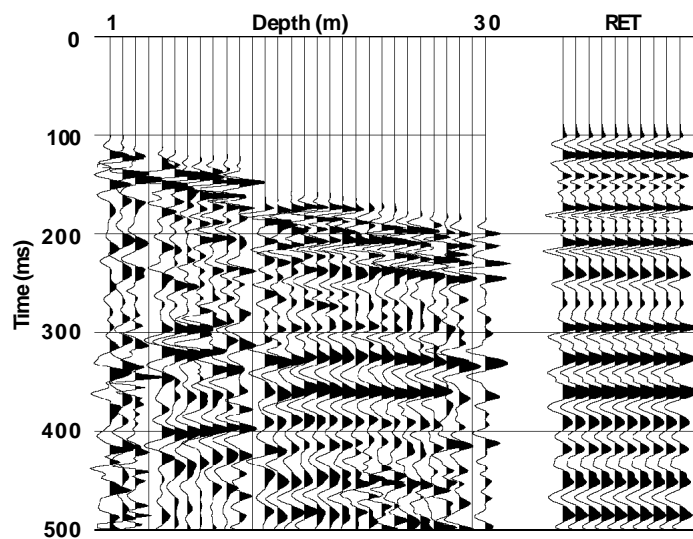
**Figure 2.16**   Aligned downgoing wavefield and RET.  Radial component (i.e. *S*-wave) data.

## Chapter 3.  Multi-component Refraction Surveys

### 3.1  Introduction

Compressional (*P*-wave) and shear (*S*-wave) seismic surveys may provide more complete information about the earth than either undertaken on its own (Stümpel et al, 1984; Hasbrouck, 1991; Stewart, 1994).  Particle motion associated with *P*-waves is in the direction of propagation of the wave, whereas for *S*-waves, particle motion is orthogonal to the direction of wave propagation.  Velocities of these waves are typically substantially lower in the very near surface than at medium or greater depths.  Considering this and Snell's law suggests that if we observe these waves as they reach the surface of the earth, the *P*-waves will have particle motion dominantly in the vertical direction and *S*-waves will have particle motion which is dominantly horizontal.  Capturing all of this information requires that we make measurements of the propagating wavefield in three orthogonal directions in order to resolve it in the most complete sense.

Three-component receivers used for these purposes most commonly contain three mutually orthogonal geophone elements.  They are employed in the field so that one component is vertical (measuring the *P*-wave), one radial or in-line with the line of the survey direction (measuring the *SV*-wave), and one transverse to the line of survey (measuring the *SH*-wave).  The conjunction between geophone components and seismic waves holds for an isotropic, homogeneous earth, with a perfectly placed seismic source and exact receiver orientation.  In the real world, there are usually variations from this most ideal case.

### 3.2  Survey Acquisition

Two refraction surveys were conducted at the University of Calgary farm site.  The first was undertaken at the same time as the RVSP survey (August, 1993), and was shot into the RVSP receiver spread.  The second was undertaken in June, 1994 at the same site.  The purpose of this latter experiment was to confirm the data obtained previously and to fill in gaps in velocity structure as determined from the RVSP and early

refraction survey.  The ground surface at the study site was flat and level over the lengths of the refraction spreads.

### 3.2.1  Cross Pattern Survey

The geophone layout for this experiment was a cross pattern, with 32 three-component OYO receivers laid out at 2 metre intervals in two lines - one east/west and one north/south.  No receiver was placed at the wellbore location.  Eight additional receivers were distributed at 4 metre intervals eastward from the eastmost cross receiver; the first of these was placed coincident with this receiver (Figure 3.1).
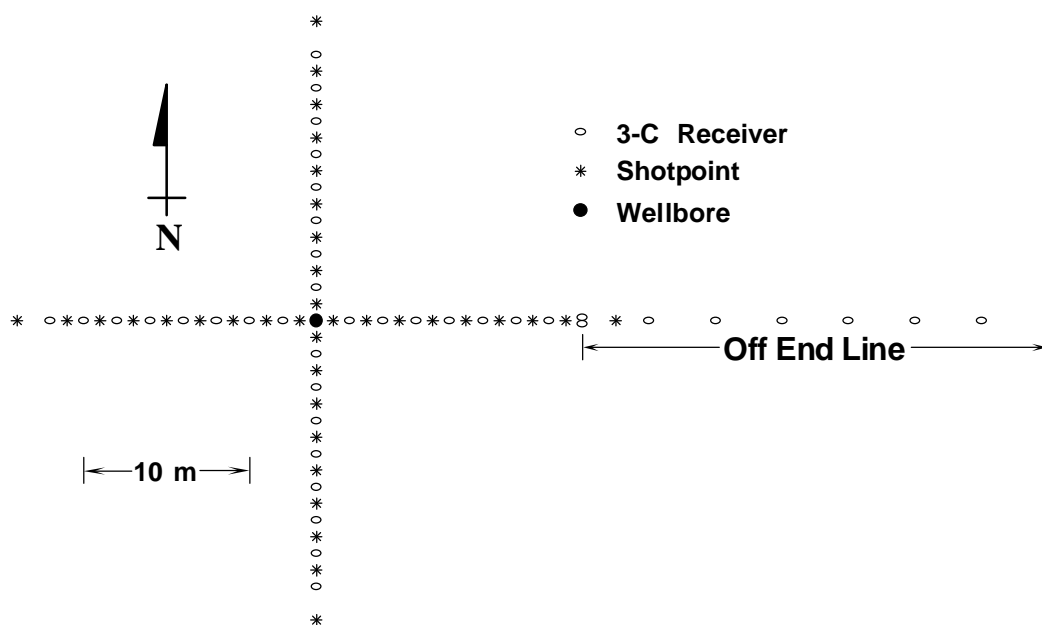
**Figure 3.1**   Cross survey diagram.  Survey layout for both surface source and RVSP experiments.

The source used was a Betsy™ Seisgun firing shots 2 metres off the end of each cross line and halfway between each adjacent pair of receivers within the cross.  This source provides most of its energy as compressional waves, and its signature is very nearly minimum phase (Beggs, 1981).  No records were obtained with shots at offsets more than 2 m off the end of the cross spread.

Data collected at the receivers within the cross were recorded using a 96 channel Sercel system sampling at 2 milliseconds, triggered by an I/O blaster. The off-end line receivers were recorded on an EG&G Geometrics StrataView 24 channel recording system sampling at 0.5 milliseconds, triggered manually. For simplicity of field setup, the vertical, radial and transverse components of each receiver were connected to adjacent takeouts. This required that the recorded trace data be sifted to form vertical, radial and transverse gathers prior to processing. The coincidence of the eastmost cross receiver and the westmost off-end receiver allowed for a time adjustment to be made to the off-end traces to bring them to the same trigger time as the cross receivers.

### 3.2.2 Multi-component Source Survey

The RVSP traveltime inversion resulted in an incomplete velocity structure for the wellbore depth interval, especially for $S$-wave velocities. The original refraction survey did not yield any useful $S$-wave information. A second refraction survey was performed in order to complete the shallow velocity profile. This second experiment was designed on the basis of the information already gathered. Modelling suggested crossover distances of about 10 and 30 m for the first two boundaries and a minimum required offset of about 200 m to observe refractions from an interpreted third boundary at a depth of 30 metres. This is based on a velocity profile as shown in Figure 3.2 - derived from the RVSP traveltime data. Shear wave velocities for those zones which did not yield a value from the RVSP were estimated by assuming $V_P/V_S = 2$.

The geophone pattern chosen for this survey was a normal in-line spread. Forty 3-C OYO geophones were laid out at 1.5 m intervals, with the line centred at the RVSP wellbore (Figure 3.3). It was roughly coincident with the east/west line of the cross spread refraction survey. While compressional wave source seismic surveys can be used to obtain shear wave information, some extra considerations are necessary (Fertig and Krajewski, 1989). The requirement is that mode conversion from $P$ to $S$ take place at some point, and that the resulting converted waves are observable. Then, only part of the travel path takes place at shear wave velocities, so a good understanding of both the

location of mode conversion and the compressional wave velocity structure, are required to resolve the shear wave velocity structure. A more direct approach is to employ a source which produces shear waves. Some part of this energy may be converted to *P*-waves, but the *S*-wave arrivals from this type of source will have higher amplitudes than converted wave arrivals from a compressional wave source.

0 m ———————————————————

$V_{P1}$ = 300 m/s

3 m ———————————————————

$V_{P2}$ = 650 m/s
$V_{S2}$ = 340 m/s

14 m ———————————————————

$V_{P3}$ = 2660 m/s

23 m ———————————————————

$V_{P4}$ = 1500 m/s
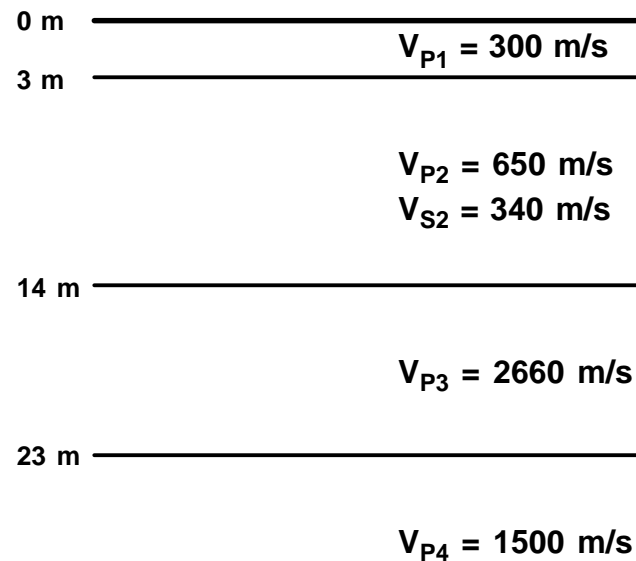
**Figure 3.2** Velocity structure from reverse vertical seismic profile (RVSP) traveltime inversion.

The second refraction survey employed two sources. The first of these was the Bison Instruments Inc. Elastic Wave Generator II (EWG II). The second source was a truck mounted bipolar *S*-wave hammer designed and constructed at the University of Calgary.

The EWG II is a *P*-wave source which uses gravity and elastic bands under tension to provide downward vertical acceleration of a mass. It is trailer mounted and towed by truck from shot to shot. The impact mass totals 250 kg and its footprint is about 0.36 m². Rapid vertical stacking of data at a single shot location allows for the relatively easy improvement of signal to noise ratios (S/N) over those obtained using a single impact. The damage inflicted by the use of this source is very slight; the only usual

indication of its employment is a shallow depression (on the order of centimetres deep) in the newly compacted soil.
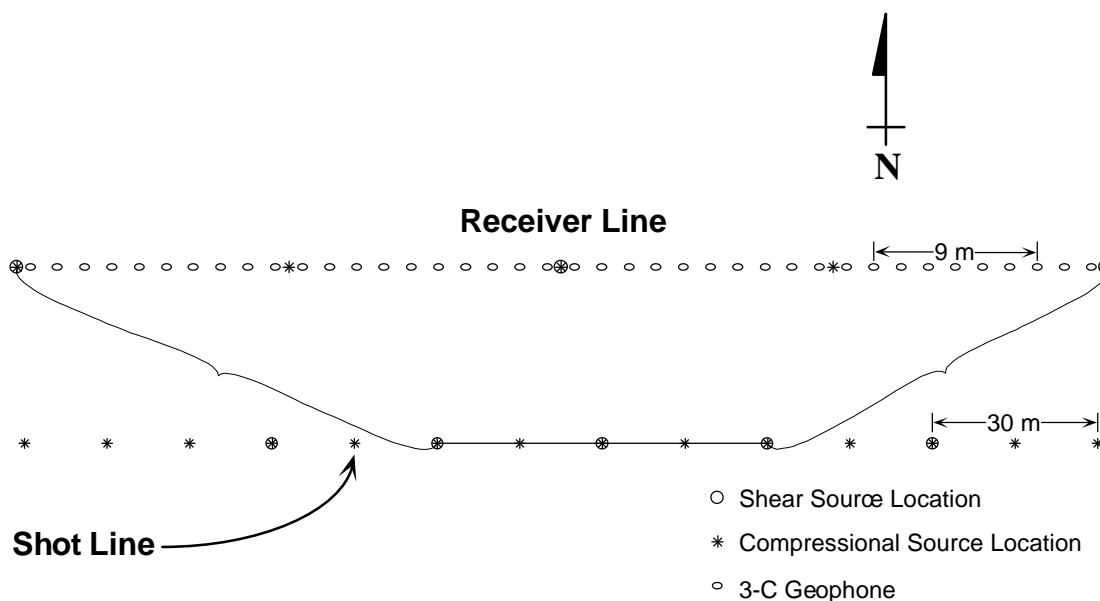


**Figure 3.3**  High resolution refraction survey field layout.

The shear wave hammer (Figure 3.4) also uses energy from gravitational acceleration to produce seismic waves.  The operational components of the source are: 1) an 80 kg hammer pivoting from a support lashed to the cable cage of a line truck, and 2) a beam lying on the earth's surface loaded with the mass of the truck.  Four strips of angle iron attached to the base of the beam ensure good coupling with the earth.  To employ the source, the hammer is raised to a fixed height and released.  The rotational path of the hammer causes it to strike the beam, imparting a shearing force on the earth.  Again, vertical stacking may be used to improve S/N.  The angle iron digs small furrows into the earth to a depth of about 5 cm.  These furrows and the impact of the line truck are the only the damage produced by this source.

The hammer may be employed in-line with the survey (*SV* mode) or perpendicular to the survey line (*SH* mode) (Helbig, 1986).  The *SH* mode is preferred as the *SV* mode produces abundant horizontally propagating *P*-wave energy which appears on the in-line

receivers.  Additionally, the *SH*-mode provides an opportunity to remove at least part of the *P*-wave energy from a final record by the following procedure.  The hammer may be suspended from either the port or starboard side of the truck.  *SH*-waves generated by an impact on one end of the beam will be 180° phase rotated from those generated by an impact on the other.  However, compressional waves will be of the same phase for either sense of the source.  Taking the difference of traces from opposite sense sources will enhance *S*-wave energy and cancel *P*-wave energy on each resulting trace (Lawton, 1990).
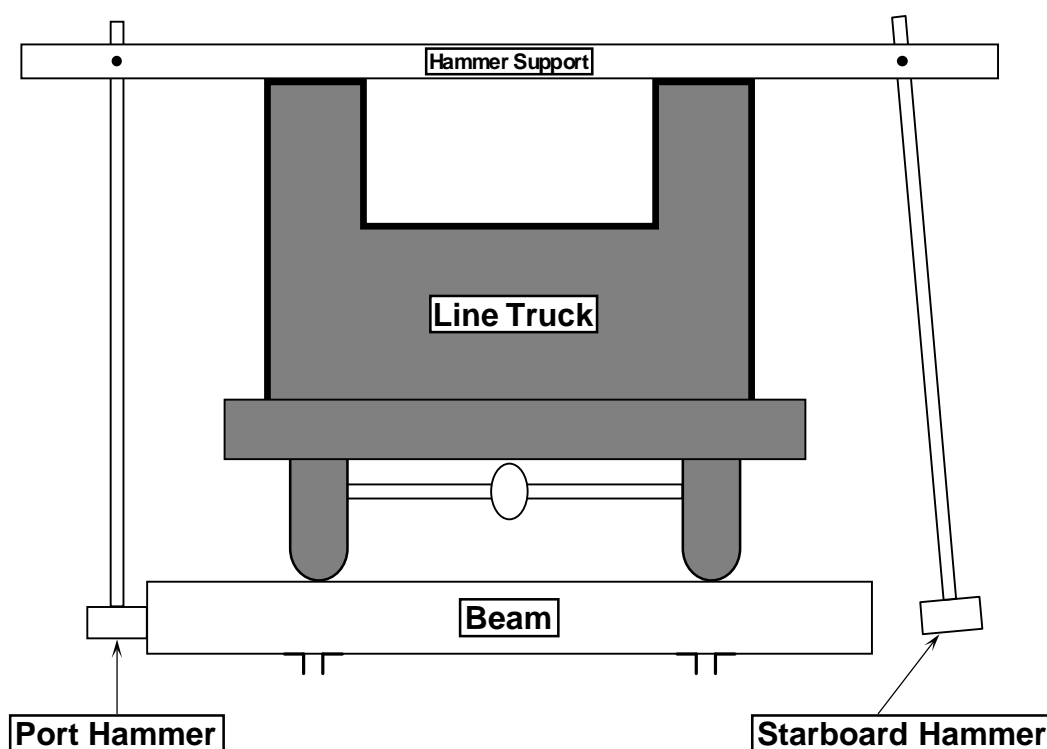
**Figure 3.4**  Shear wave hammer source.

Data collected in this second refraction survey were recorded using a 120 channel OYO DAS-1 recording system, triggered by a geophone planted beside the beam.  Again, the vertical, transverse and radial component for each receiver were recorded at adjacent trace locations for ease of field setup.  Gathers for each orientation were obtained in processing by sifting to 40 trace common shot gathers.

### 3.3  Data Processing

### 3.3.1  Cross Survey

A vertical channel record obtained by a shot 15 m west of the well location is displayed in Figure 3.5.  These data have had an AGC applied to them with window length 200 ms, and are amplitude trace equalised.  The traces are plotted in proper offset location with the exception of trace 17.  Trace 17 is the Geometrics recorded trace coincident with cross line trace 16 and is plotted slightly out of place in order that the two traces don't overlie each other.  A more ready comparison of the two traces can be made using Figure 3.5b.  Traces 16 and 17 are very nearly identical.  No AGC or trace equalisation has been applied to these data.  The data recorded using the Geometrics instrument were sampled at 4 times the frequency of those recorded by the Sercel instruments.  For plotting purposes, the Sercel traces have been resampled to 0.5 ms using standard seismic data processing software (ProMAX).

### 3.3.2  Multi-component Source Survey

The data processing for this survey is similar in simplicity as was that used for the cross survey.  Figures 3.6 shows records obtained using the EWG II and shear hammer sources respectively.  The processing applied to both gathers has been a simple sift to the appropriate component (vertical for the EWG II source and transverse for the shear hammer) followed by a 200 ms window AGC and then trace equalisation for display.  In order to pick the first breaks more precisely, the records were windowed over very short trace and time intervals.  The procedure was to make coarse picks along straight lines, then zoom in tightly to the vicinity of those picks and refine them.  The precision obtained in this way is fine enough that the remaining error is best attributed to error in locating the receivers rather than in timing.
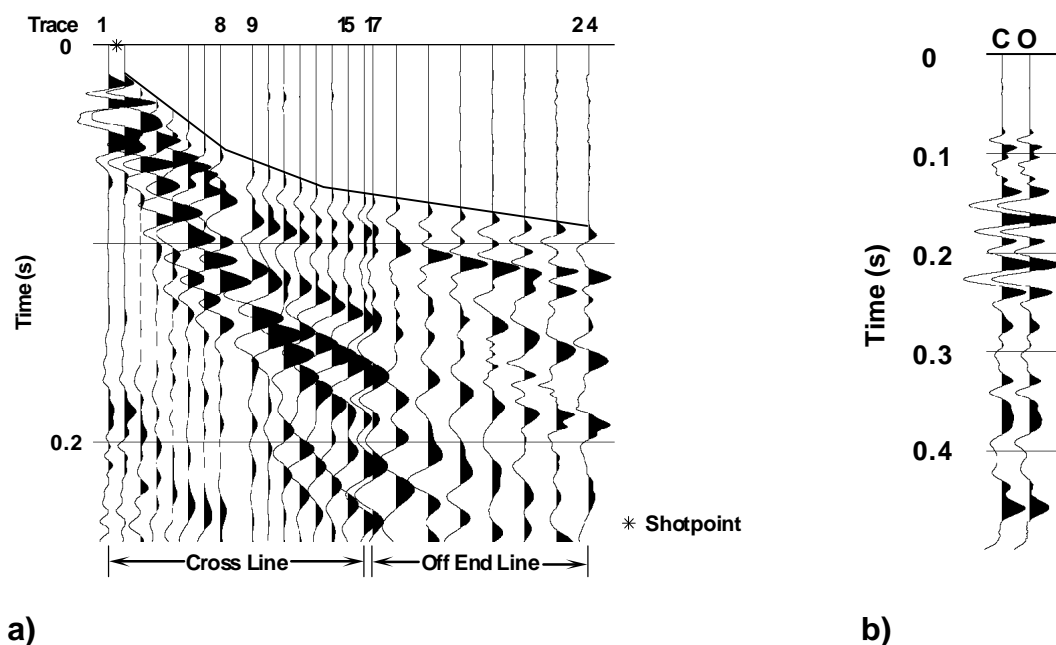
**Figure 3.5**    Vertical channel record - cross survey.   The first arrivals are shown highlighted.  a) Three velocity zones are apparent on the record: 1) Trace 1-8, 2) Trace 9-14, 3) Trace 15-24.   b) Comparison of traces obtained from adjacent receivers at 16 metres offset from the RVSP wellbore.  The source point was at 15 metres offset the wellbore in the opposite direction.  **C** - cross line trace.  **O** - off end line trace.

## 3.4  Interpretation

### 3.4.1  Methods

In its simplest form, refraction interpretation considers the earth to be comprised of two or more horizontal layers.   The layers are expected to be homogeneous and isotropic in their acoustic properties.  The geometry and mathematics required to interpret an earth model of this type are very simple, namely the slope/intercept approach which requires one shot into a spread and provides depth and velocity information only at the location of the shot.   Provided that the assumptions hold, this is adequate to define the velocity structure locally.
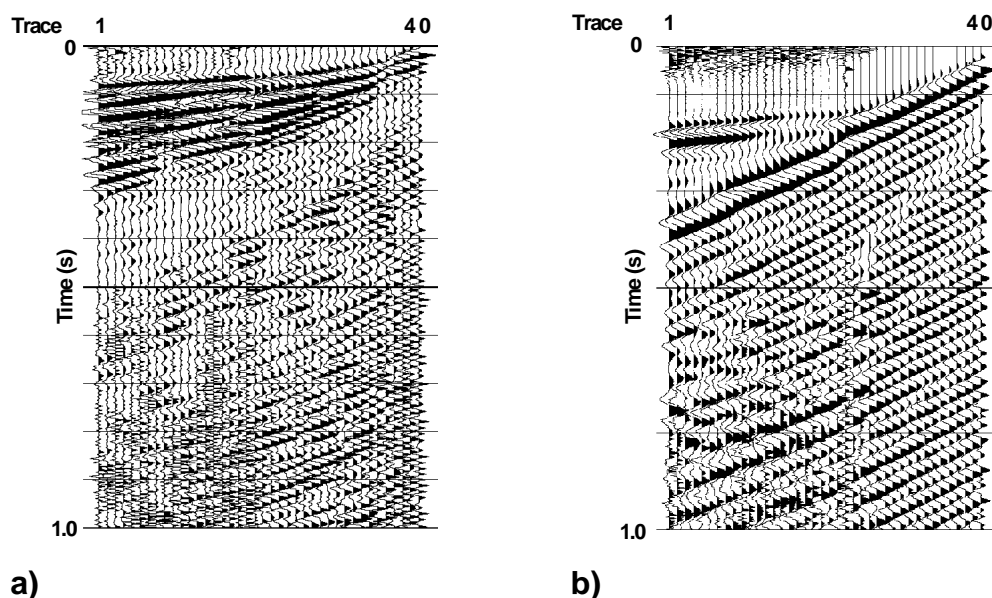
**Figure 3.6** a)   EWG II vertical component gather; 200 ms AGC applied.  b) Shear hammer transverse component gather; 200 ms AGC applied.

Improved lateral resolution can be obtained by acquiring more data, especially by placing sources at both ends of the receiver line.  This affords the opportunity to compare traveltimes to a specific receiver from shots arriving from more than one location and leads to a variety of inversion schemes based on the differences in those traveltimes.  Two of these schemes were investigated for use in the present work; the generalised reciprocal method or GRM (Palmer, 1980) and the plus-minus method (Hagedoorn, 1959).

The GRM (Figure 3.7) is an attempt to identify that pair of receivers which record arrivals refracted from very nearly the same location on the refracting boundary.  To do this one first constructs two sets of curves - the velocity analysis function, and the generalised time-depth function.  These sets of curves are used to choose which XY spacing (receiver pair interval) suits the stated object.  If the refractor exhibits significant structure, some of the velocity function curves will deviate significantly from a straight line.  There will be similar variation in the generalised time-depth curves.  The proper choice of XY value is that which causes the velocity function to most closely

approximate a straight line and the generalized time depth to exhibit the most detail (Palmer, 1981).  These criteria result from an averaging effect inherent in the calculation of the two curves.  As the appropriate XY value is reached, the traveltime contribution for both is derived from a smaller portion of the refractor.  Undulations of the investigated surface will therefore be less likely to contribute unwanted variation to the velocity function and will not be smeared over as large a segment of the generalized time-depth curve.  When the most correct choice of XY value is made, depths are readily calculated.
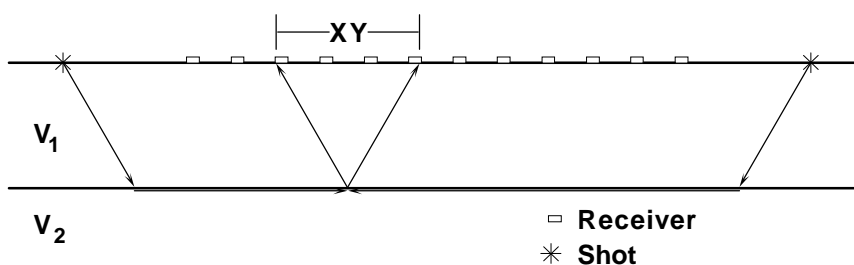


**Figure 3.7**   Illustrates the shot/receiver geometry for the generalised reciprocal method of refraction interpretation.

The usefulness of the GRM is impaired by the requirement that the refractors of interest contain some structural relief to properly determine the optimum XY value.  That criterion does not apply to the plus-minus method (Figure 3.8), which also uses reversed shots to improve the lateral resolution of refraction surveying.  It assumes that the refracted wave arrivals from shots offset in opposing directions (termed forward and reverse for convenience) to a receiver leave the refracting surface from very nearly the same lateral location.  For any receiver which records refracted arrivals from forward and reverse directions, one can determine refractor velocity and depth below the receiver location.  Judicious application of these parameters outside of the plus-minus window[3.1] allows one to calculate depths at other receiver and shot locations.

---

[3.1] This window is comprised of the offset range over which critically refracted arrivals from opposite shots are recorded.
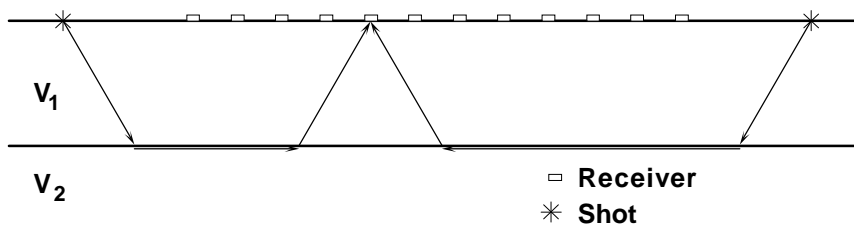
**Figure 3.8** Illustrates the shot/receiver geometry for the plus-minus method of refraction interpretation.

These methods may be improved upon by careful attention to data acquisition. If more shots are taken - typically in the centre of the spread and offset some distance from either end - the traveltime curves for each boundary investigated can be filled in for the entire receiver line (Lankston, 1990). This technique is referred to as "phantoming" and simply requires shifting long offset traveltimes to match near offset arrival times to produce a complete reciprocal suite of refraction data (Lankston and Lankston, 1986). The plus-minus or GRM interpretation schemes can be used to interpret the phantomed curves.

### 3.4.2 Cross Survey

Figure 3.5 shows clear, readily interpretable first arrivals on all traces. The source is impulsive, so first breaks are identified as the first motion above background levels on each trace (i.e. assumption of a minimum-phase wavelet). Three distinct layers are apparent from the three distinct slopes of these arrivals (indicated by lines on Figure 3.5). Abundant ground roll is also evident but does not interfere with the first arrival traveltime picking.

The zero offset time intercept for the first layer of any refraction survey should be 0 seconds. Any other value signifies a problem with recording or triggering or possibly the presence of an unidentified shallow layer. There is such a problem with the data presented in Figure 3.5. The time intercept for the first layer here is about 10 ms and it is unreasonable to attribute this to an unidentified layer. The identified first layer velocity of about 330 m/s is very close to the speed of sound in air. The fastest shallower layer

that could be accommodated by the data would be a 0.4 m thick layer with the improbable $V_P$ = 80 m/s. The delay is postulated to result from an approximately 10 ms time advance in triggering which is consistent from record to record (i.e. pre-trigger). Such an occurrence may be the result of a discrepancy between the trigger time electronically relayed to the recording unit and the time at which the shotgun slug strikes the earth. The average advance for all records is 11 ms. All records were adjusted for this time delay before interpretation. The raw traveltimes (prior to the time correction of -11 ms) for both arms of the cross are shown in Figures 3.9 and 3.10.

Thirty-five refraction records were obtained in this phase of the study. The offsets used were such that a maximum plus-minus window of 4 stations was observed for the reciprocal records obtained from the farthest separated east and west source points. The farthest separated north and south source points provide a plus-minus window of only 2 stations. This window only contains arrivals from the first refracting surface. A second refractor is apparent on the east/west lines only for shot/receiver distances beyond 28 metres. Depth estimates for this last event are only obtainable from single ended records and so have been obtained using the slope/intercept procedure. The compressional wave velocity structure as determined by this survey is shown in Figures 3.11 and 3.12. It was obtained by a combination of slope/intercept interpretations for each shot (considering dip where possible).

The maximum shot/receiver offset for the north/south line is 34 metres; for the east/west line it is 62 metres. Minimum offset required to observe refracted arrivals from the second interface is about 28 metres. To properly identify this event, one must observe the arrivals at several receiver locations. The result is that refracted arrivals from the third layer are not present on most records for the north/south line, but do appear on many of the east/west line records. Hence the velocity structure shown for the east/west line extends deeper into the earth than that for the north/south line.
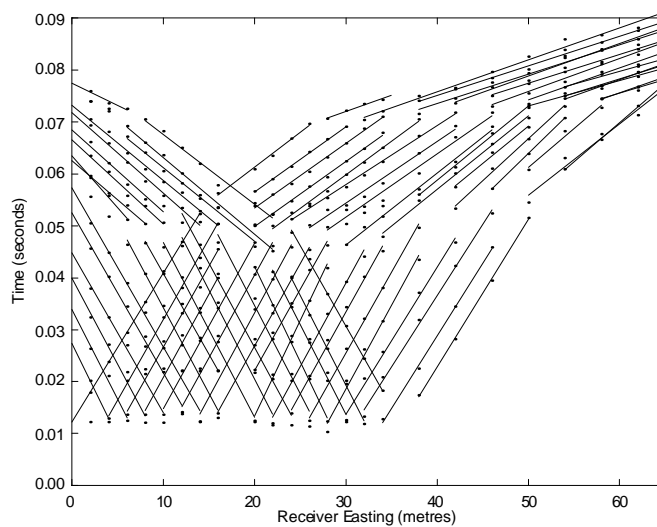
**Figure 3.9**  Compressional wave traveltimes - cross survey east/west line.  First break picks with best fit lines for each velocity arrival for each shot record.
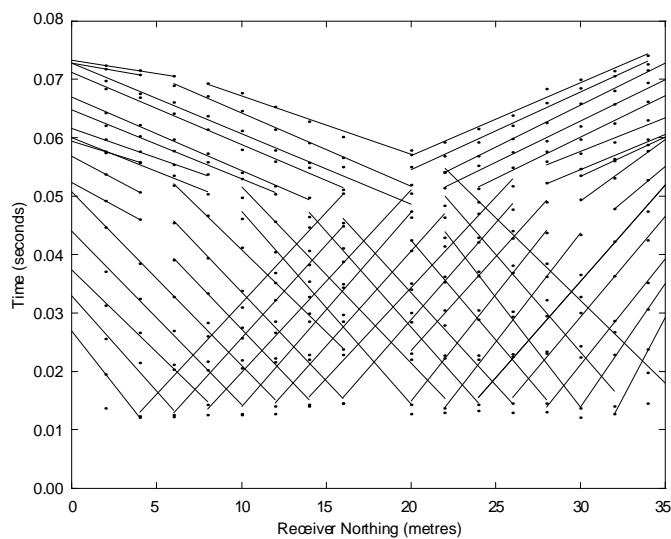


**Figure 3.10**  Compressional wave traveltimes - cross survey north/south line.  First break picks with best fit lines for each velocity arrival for each shot record.
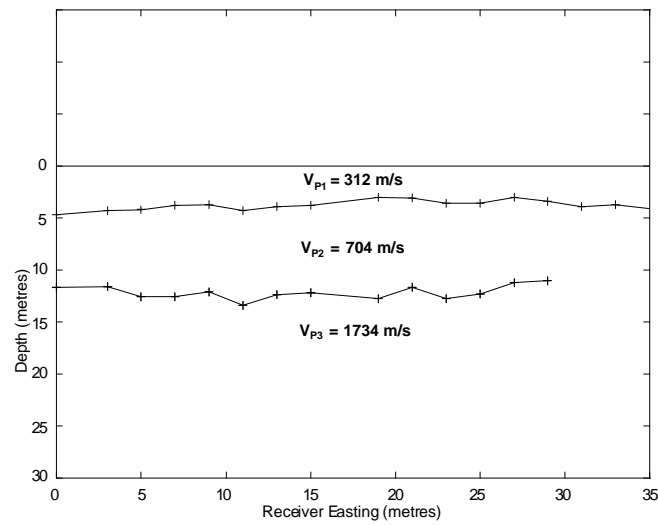
**Figure 3.11**   Interpreted *P*-wave velocity structure - cross survey, east/west arm of cross.
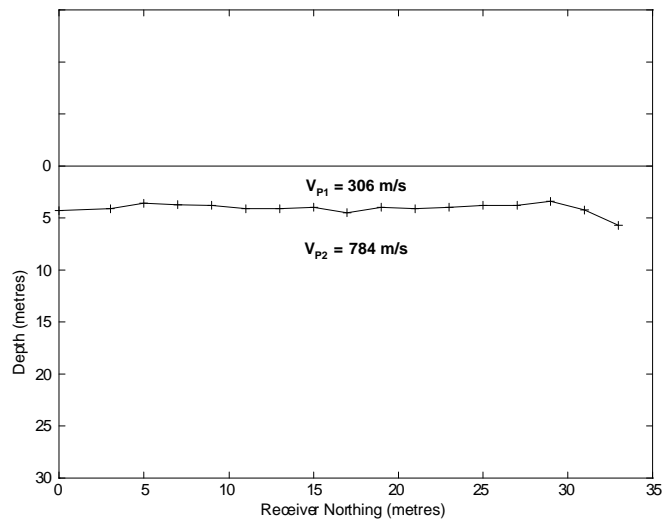


**Figure 3.12**   Interpreted *P*-wave velocity structure - cross survey, north/south arm of cross.

### 3.4.3  Multi-component Source Survey

Three distinct segments are visible on the *P*-wave record shown in Figure 3.6 a), whereas only two are evident on the *S*-wave record in Figure 3.6 b).  Traveltime curves for these experiments (Figures 3.13 and 3.14) clearly show that three layers are defined by the *P*-wave survey but only two for the *S*-wave survey.  A more dense shotpoint interval than that for the cross survey allowed a full suite of reciprocal curves to be constructed for two refracting surfaces for the *P*-wave data, and one for the *S*-wave data.  For the purposes of this discussion, curves for which the traveltime increases with increasing easting values will be referred to as forward curves, while those for which traveltime decreases with increasing easting values are termed reverse curves.

One of the major reasons for performing this survey was to obtain longer offset information.  This was expected to extend the depth of investigation.  The longest offsets available in the cross survey were 62 m (a single-sided record, using the off-end line).  The multi-component source survey included shots up to 135 m offset to the west and 120 m offset to the east.  For such a geometry and assuming a fourth *P*-wave layer with velocity of 3200 m/s (typical weathered Porcupine Hills velocity), the minimum depth to the top of the fourth layer is 47 metres.

The traveltimes were phantomed to obtain reciprocal traveltime curves which represent the theoretical traveltimes that would be obtained at each receiver location for each refractor investigated.  These are purely theoretical over some portions of the line - some of the phantomed arrivals occur at less than the critical distance.  Phantoming allows one to obtain a refracted traveltime value in regions where one would not otherwise be obtainable (i.e. at offsets less than the cross-over distance).  The reciprocal traveltimes thus obtained are well suited to a variety of interpretation schemes.
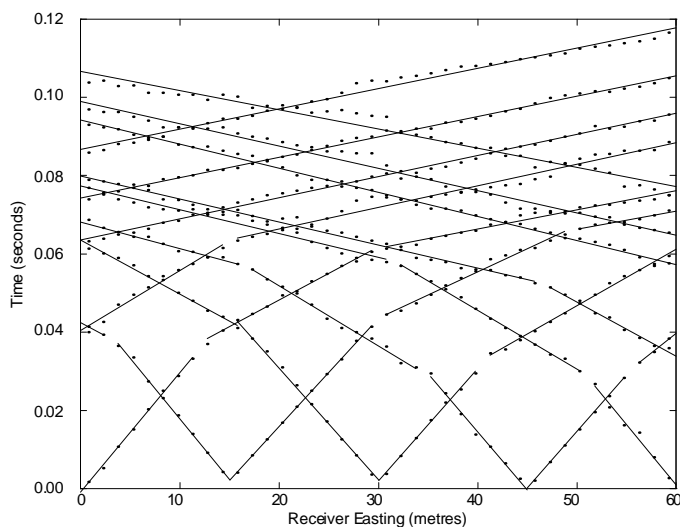
**Figure 3.13**   Compressional wave traveltimes - multi-component survey.  First break picks with best fit lines for each velocity arrival for each shot record.
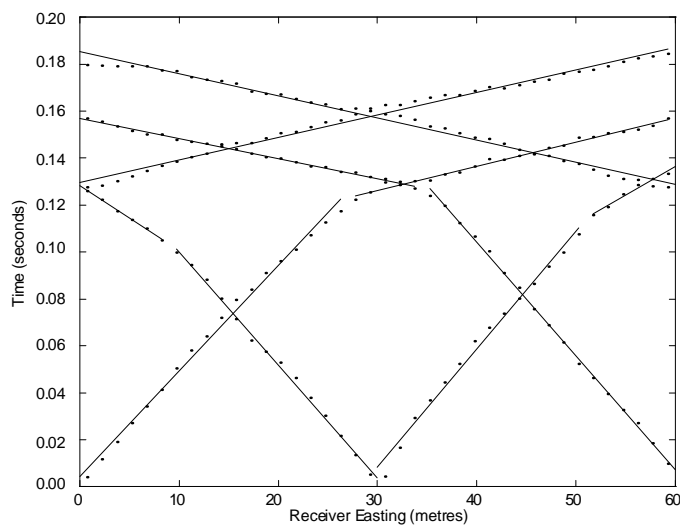


**Figure 3.14**   Shear wave traveltimes - multi-component survey.  First break picks with best fit lines for each velocity arrival for each shot record.

Two different interpretation schemes (GRM and plus-minus) were applied to these data.  Figure 3.15 presents the results of the analysis of the *P*-wave data.  The first refractor (at about 4 m depth) shows close agreement with the results obtained from the

cross survey. The second refractor surface was estimated in three different ways. The additional set of depths is for an interpretation using GRM analysis in which the upper two layers are combined into a single layer. In this method, an average velocity to the refractor is used to eliminate the need for consideration of individual upper layers. This approach is most useful in the event that a hidden layer or velocity inversion is suspected, and appears to produce a result which is similar to the more complete interpretation.

Figure 3.16 shows the result of the *S*-wave traveltime analysis. The upper refractor evident in Figure 3.15 is not apparent here. The only refracting surface in evidence is close to the level of the second *P*-wave refractor. Comparison of the two depth interpretations suggests that refractor 1 represents a change in acoustic impedance largely controlled by fluid content, whereas refractor 2 is probably a lithologic boundary. Figure 3.17 compares the plus-minus depth interpretation for the *P*-wave and *S*-wave surveys. The match between the two is not exact for the second refractor, but is very close (Table 3.1). The *S*-wave depth profile appears to image the long wave-length component of the *P*-wave depth profile. The velocities determined from the refraction surveys are reasonable values for the lithologies known in this area (undersaturated and saturated tills resting on gravels).

**Table 3.1**   Summary of *P*-wave and *S*-wave depths and velocities.

| | $V_P$ (m/s) | $\bar{d}_P$ (m) | $V_S$ (m/s) | $\bar{d}_S$ (m) | $V_P/V_S$ |
|---|---|---|---|---|---|
| Layer 1 | 339±6 | 3.6±0.5 | 220±4 | - | 1.5±0.1 |
| Layer 2 | 713±6 | 12.2±1.3 | 220±4 | 11.4±0.8 | 3.2±0.1 |
| Layer 3 | 1750±30 | - | 1046±14 | - | 1.7±0.1 |

Errors in the depth determination arise largely from errors in velocity estimation and approximation of the reciprocal time. The first break times can be picked to within 0.5 milliseconds; the contribution of timing errors to depth errors are minimal (less than 0.1 metres) and are overwhelmed by the velocity error. Velocity and reciprocal times are

both obtained by least squares approximation and the error values given are those of standard error of the estimate.   Offset measurements are quite accurate and contribute little to the overall errors.
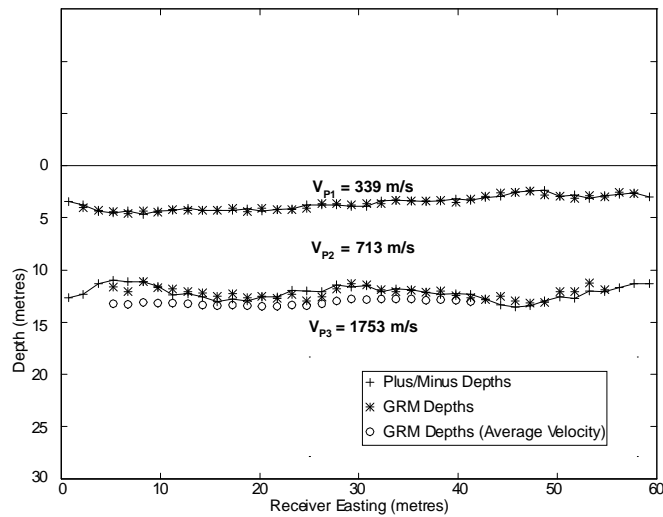


**Figure 3.15**   *P*-wave refraction interpretation - multi-component survey.
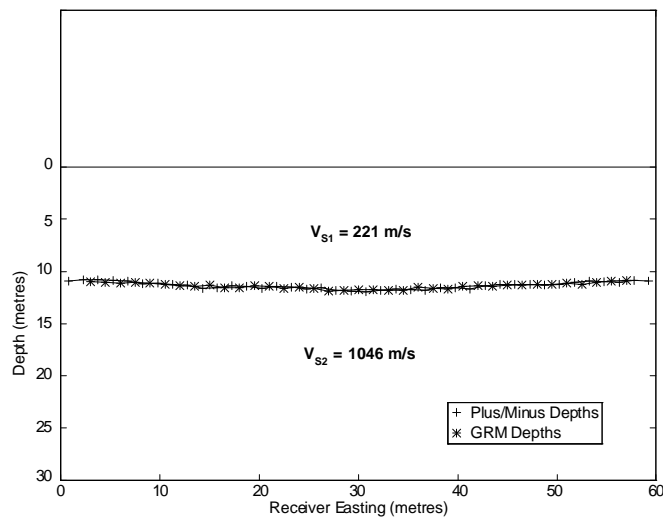


**Figure 3.16**   *S*-wave refraction interpretation - multi-component survey.

Variations in values of $V_P/V_S$ in the near-surface can be much greater in the shallow earth than at depth because fluid saturation is much more variable and porosity may be much greater at shallow depths. The *S*-wave velocity will be unaffected by variations in fluid volume, while the *P*-wave velocity may be significantly affected. This is clearly the case in the layer 1/layer 2 transition which is apparent on the *P*-wave data and transparent for the *S*-wave. The $V_P/V_S$ variation observed here is significant if less dramatic than other investigators have shown. Stümpel et al. (1984), Wiest and Edelmann (1984), and Lawton (1990) show $V_P/V_S$ variations in similar geological materials at similar depth ranges (Table 3.2). Brabham and Goulty (1988) show that in areas where the water table is well below the investigated zone, $V_P/V_S$ variation is much smaller. The relatively small increase at the farm site suggests that the abrupt increase in $V_P/V_S$ ratio is not indicative of the water table proper, but of a zone of relatively high water saturation, perhaps a manifestation of climactic effects in the extreme shallow zone. This is especially likely as the higher porosity gravels underlying this zone exhibit relatively low $V_P/V_S$.

**Table 3.2** $V_P/V_S$ estimations from several investigators.

|  | $V_P/V_S$ (Stümpel) | $V_P/V_S$ (Wiest and Edelmann) | $V_P/V_S$ (Lawton) |
| --- | --- | --- | --- |
| Unsaturated | 2.0 | 3.3 | 2.0 |
| Saturated | 10.0 | 8.0 | 8.3 |
| Bedrock | 4.9 | 5.3 | 2.4 |
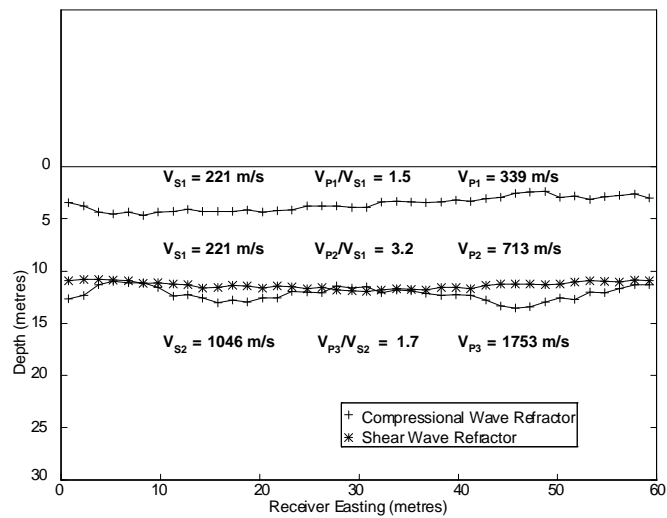
**Figure 3.17** Comparison of depth sections shear and compressional wave data - multi-component survey.

## Chapter 4.   Electrical Geophysical Methods Tested

### 4.1   Introduction

Vertical electrical soundings (VES), fixed frequency electromagnetic induction surveys (FEM), and ground penetrating radar (GPR) surveys were all undertaken in an effort to observe and record the local earth electrical structure at and nearby the farm site. The FEM surveys provide a data set which effectively characterises the variation of electrical conductivity laterally, but quantitative depth information is difficult to obtain from them (McNeill, 1990).   The VES provide good local estimates of the earth conductivity in depth, but take a significant amount of time to acquire for each sounding (on the order of 3 hours per sounding).   Inverting VES data for conductivity structure also introduces the equivalence problem; i.e. an infinitude of different earth models may fit the same sounding data (Ward, 1990).   Some of these models may be eliminated as they are not geologically reasonable, but no single unequivocal solution can be produced.   GPR data are acquired rapidly and may provide useful depth information, but are only applicable in locations where the electrical conductivity of the near-surface falls in a limited range - the GPR signal is attenuated rapidly in media of high electrical conductivity[4.1].   This combination of techniques was chosen in order to provide some redundancy for comparative purposes and so that the limitations of one technique might be counter-balanced by a strength in another.   Other techniques (micro-gravity studies, magnetic field measurements, resistivity profiling, etc.) were dismissed as being expensive to perform, difficult to interpret and unlikely to add significantly to an understanding of the local geology.

---

[4.1] Penetration depth is roughly: $d_{max} < \dfrac{35}{\sigma}$, where $d_{max}$ is maximum depth in metres and $\sigma$ is conductivity in mS/m (Davis and Annan, 1989).

## 4.2   Vertical Electrical Sounding

### 4.2.1   Data Acquisition

A Schlumberger array vertical electrical sounding was performed at the farm site during May of 1995.  The centre point for the sounding was the RVSP wellbore, with the array laid out in an east/west orientation.  A low frequency Scintrex IP transmitter was the current source, and resulting electrical potentials were measured with a multi-meter.  The Schlumberger array (Figure 4.1) consists of an interior potential dipole (termed MN), and an exterior current dipole (termed AB).  Both dipoles are arrayed symmetrically in a straight line running through the sounding centre point (Telford et al., 1976).  The potential dipole was held constant at 1 m for the first seven AB spacings and then increased to 10 m for the next seven.  AB spacings were chosen to provide six readings per decade of increased separation, spaced evenly on a logarithmic scale.  Acquisition parameters are compiled in Table 4.1.
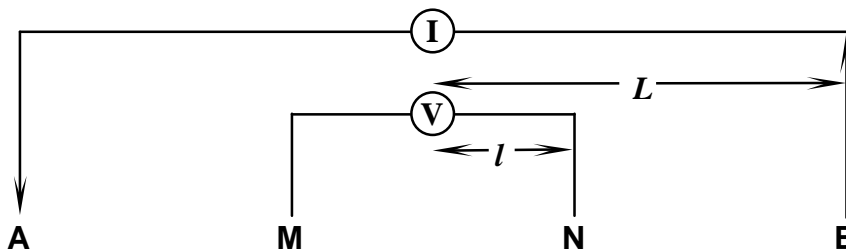


**Figure 4.1**   Schlumberger DC resistivity sounding array.  Geometrical arrangement of current electrodes (A and B) and potential electrodes (M and N).

During the acquisition of Schlumberger sounding data, the measured potential decreases as the AB spacing increases.  Eventually this value will decrease to the point where ambient electrical noise overwhelms the broadcast signal.  At this point, expanding the potential dipole will improve S/N and the current dipole may again be lengthened.  One of the results of this tactic is that apparent resistivity ($\rho_a$) values calculated for the same AB spacing at different MN spacings are rarely the same.  The difference (or "clutch" on the sounding curve) is attributed to local heterogeneity in electrical properties

(Ward, 1990). The values determined using small MN spacings were adjusted to match the large MN spacing values at an overlapping point. This adjustment is preferred as the larger MN spacings will be less affected by extremely localised conductivity variations.

### 4.2.2  Data Processing and Interpretation

The data processing for this type of survey is minimal. The electrical potential difference ($\Delta V$) and applied current ($I$) are measured in the field and used to calculate apparent electrical resistivity ($\rho_a$), given the electrode array geometry. For the Schlumberger array, the apparent resistivity is computed by:

$$\rho_a = \frac{\pi L^2}{2l}\left(\frac{\Delta V}{I}\right)$$

where $L$ is half the current dipole spacing and $l$ is half the potential dipole spacing.

These data are interpreted using either a curve matching procedure or by applying a computer-based inversion scheme. In the curve-matching method, theoretical curves are compared with the reduced data until a close match is obtained. The earth resistivity and depth are then calculated from parameters for the theoretical curves. Computer analysis requires that the interpreter estimate number of layers and approximate resistivity values from the plotted data. A theoretical curve is derived from the estimated parameters and plotted against the field data. This then forms an iterative process, where the interpreter varies the input parameters to obtain a close match of the data. Once the result is satisfactory, the input parameters are taken to represent the true earth parameters. The inversion software that was used for the present analysis (Interpex' RESIX) takes the first parameter estimation and uses a least squares approach to attempt to minimise the difference between the input data and the theoretically derived curve. No earth parameters were fixed to force the inversion result. The results are shown in Figure 4.2 and listed in Table 4.2.

**Table 4.1**  Vertical Electrical Sounding - Raw Data

| MN (m) | AB (m) | Potential (V) | Current (A) | $\rho_a$ ($\Omega$m) |
|--------|--------|---------------|-------------|----------------------|
| 1 | 2 | 11.195 | 0.70 | 50.24 |
| 1 | 3 | 3.383 | 0.61 | 39.20 |
| 1 | 4.4 | 1.525 | 0.57 | 40.68 |
| 1 | 6.4 | 1.250 | 1.00 | 40.21 |
| 1 | 9.2 | 0.764 | 1.14 | 44.55 |
| 1 | 13.6 | 0.182 | 0.56 | 47.21 |
| 1 | 20 | 0.020 | 0.14 | 44.32 |
| 10 | 20 | 1.940 | 1.04 | 58.60 |
| 10 | 30 | 0.972 | 1.29 | 53.23 |
| 10 | 44 | 0.541 | 1.30 | 63.22 |
| 10 | 64 | 0.169 | 0.64 | 85.62 |
| 10 | 92 | 0.106 | 0.61 | 114.97 |
| 10 | 136 | 0.100 | 0.97 | 150.84 |
| 10 | 200 | 0.069 | 1.12 | 193.52 |

**Table 4.2**  VES Inversion Results.

| Zone | Depth (m) | Resistivity ($\Omega$m) | Conductivity (mS/m) |
|------|-----------|-------------------------|---------------------|
| 1 | 0-0.3 | 139.5 | 7.2 |
| 2 | 0.3-1.8 | 41.3 | 24.2 |
| 3 | 1.8-3.2 | 137.2 | 7.3 |
| 4 | 3.2-12.5 | 33.9 | 29.5 |
| 5 | 12.5+ | 503.3 | 2.0 |
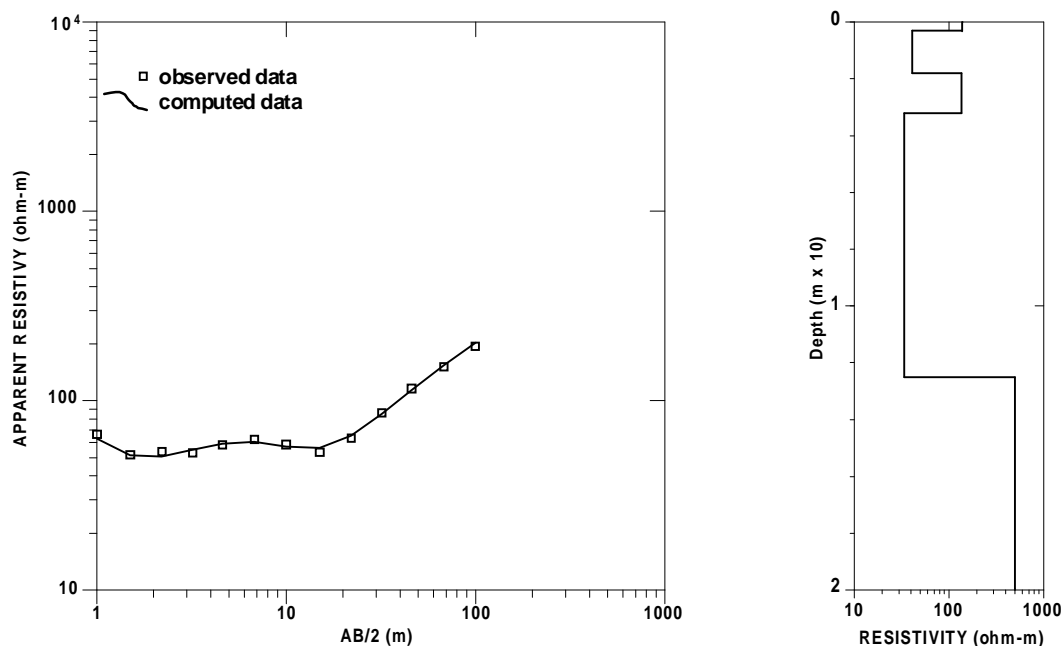
**Figure 4.2**  VES curves and inversion derived resistivity model.

The interpreted resistivity depth model suggests two broad electrostratigraphic layers.  The upper layer (zones 1, 2, 3 and 4 in Table 4.2) is of relatively moderate resistivity, and occurs from 0 to 12.5 metres depth.  The lower layer (zone 5 in Table 4.2) is relatively higher in electrical resistivity; its base is not identified.  This conductivity structure is consistent with clay-rich till overlying gravels.  Generally, finer-grained materials (especially mineralogical clays) are lower in resistivity than are coarse grained materials (McNeill, 1980*a*).  The upper electrical layer is comprised of several zones suggestive of small scale lateral and vertical lithological variations within the tills.  The higher resistivity values are attributed to a local accumulation of more coarse-grained material (zone 3) and to an unsaturated zone immediately at the surface (zone 1).  Zone 3 is probably very localised, while zone 1 is broadly distributed but contributes little to the gross electrical structure as it is extremely thin.  Small scale geoelectrical variations (geological heterogeneities of limited size) at shallow depths are much more readily identified by this method than are small scale variations at deeper levels.  For consistency in interpretation, it is best to pay closest attention to the longer wavelength features.

## 4.3 Fixed Frequency Electromagnetic Induction Surveys

### 4.3.1 Introduction

The electromagnetic methods are a variety of techniques which use measurement of a time-varying electromagnetic field to investigate variations in the earth's electrical structure. The source of this field may occur naturally, may be supplied for the survey, or one may take advantage of existing, remote, man-made fields (i.e. communications signals). These techniques apply largely to the shallow earth and are most suited to investigation of anomalies of relatively high conductivity in a more resistive host. Conductivity anomalies may rise from variation in clay content, local concentrations of other high conductivity minerals, pore fluid conductivity, pore fluid volume, and temperature (McNeill, 1990).

For very shallow investigations, a local, low-power source is useful. Such a source can be readily controlled to produce a signal of constant frequency and phase. The method of choice uses two coils in one of several common geometries; an alternating current is passed through a transmitting coil (Tx) which broadcasts a time-varying magnetic field (Figure 4.3), a known voltage is thereby induced in the receiving coil (Rx). Any deviation from the anticipated voltage in the receiving coil is attributed to mutual inductance between the coil and an earthbound body of anomalous conductivity (Telford et al., 1976).

The instruments chosen for this portion of the study were the Geonics Limited EM31 and EM34-3 Ground Conductivity Meters. These instruments are fixed frequency electromagnetic induction devices. The EM31 operates at 9.8 kHz and the EM34-3 at 6.4 kHz (10 m separation), 1.6 kHz (20 m separation), and 0.4 kHz (40 m separation). The depths of investigation afforded by the instruments can be varied by changing the instrument height and orientation and, for the EM34-3, the coil separation (frequency must be changed with coil separation). These instruments are specifically designed to measure ground conductivity under the special operating condition of low induction number. Induction number is defined as the ratio of the intercoil spacing to the electrical

skin depth of a homogeneous half-space. By choosing frequency of operation and assuming a limited upper value of measured conductivity (about 100 mS/m) such that induction number is much less than unity, the ratio of the secondary magnetic field to the primary at the receiving coil is a linear function of half-space conductivity (McNeill, 1980*b*).

The EM31 is a single-person portable instrument. It contains a transmitting and receiving coil at opposite ends of a 3.7 metre long fibreglass boom. A digital meter on the instrument provides a direct reading of apparent conductivity and of the in-phase ratio of the primary to the secondary magnetic field in parts per thousand. Readings can be recorded immediately in a field book or can be digitally captured in a recording device for later transfer to a microcomputer.
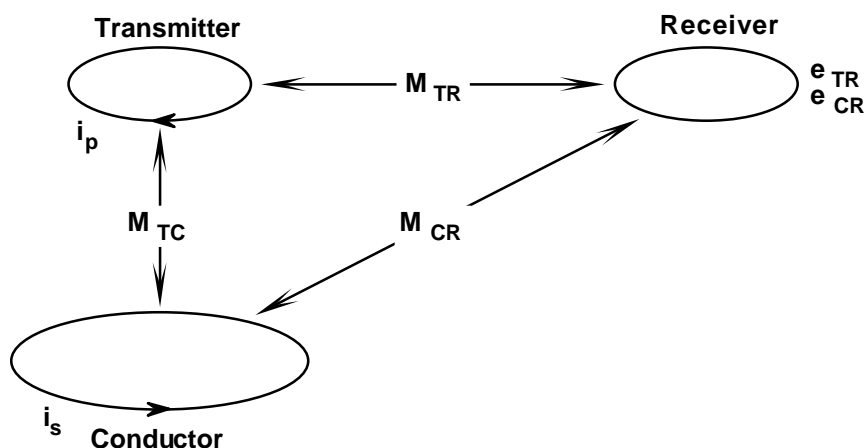


**Figure 4.3** Electromagnetic induction coil equivalent circuit geometry. Illustrates mutual inductances (M) and currents (i) involved and resulting emf (e) at the receiving coil.

The EM34-3 requires two people for its operation. It consists of transmitting and receiving coils (each about 75 cm in diameter) connected by one of a 10, 20, or 40 metre long cable. The operators each carry a coil and a box containing the controlling electronics. Intercoil distance is calculated internally by measuring the in-phase signal, allowing the operators of the equipment to rapidly establish a defined coil separation at

each measurement station. Readings of apparent conductivity are presented on the receiving console and can also be recorded digitally.

The normal mode of instrument operation for the EM31 (its carrying position) orients the coils so that their axes are vertical. The dipoles are rotated to the horizontal by turning the instrument on its side. EM34-3 carrying position arranges the coil axes horizontally. Laying the coils flat on the ground arranges the dipoles vertically. Dipole alignment is an important consideration as depth of investigation is directly affected - effective investigation depth is approximately double for the vertical dipole as compared to the horizontal. The depth of investigation for any instrument is arbitrarily chosen as the depth for which the conductivity contribution from all deeper material provides about 30% of the response (McNeill, 1980*b*). The effective exploration depths for the common operation modes are provided in Table 4.3. All instrument operating modes were used at the farm site with the exception of the 10 m horizontal dipole EM34-3 reading and the 1 m elevation EM31 horizontal dipole reading.

**Table 4.3**  Effective exploration depths for the EM31 and EM34-3 Conductivity Meters

| | | Horizontal Dipoles | Vertical Dipoles |
|---|---|---|---|
| Instrument height (m) | Intercoil spacing (m) | Depth of Exploration (m) | |
| 0 | 3.7 | 3 | 6 |
| 1 | 3.7 | 2 | 5 |
| 0 | 10 | 7.5 | 15 |
| 0 | 20 | 15 | 30 |
| 0 | 40 | 30 | 60 |

### 4.3.2  Data Acquisition

Fixed frequency electromagnetic induction data were obtained at the farm site over a grid centred on the RVSP wellbore. The grid was comprised of five lines running east/west and one north/south. The east/west lines were placed at 0, 20, 40, 60 and 75 metres north. These were all 100 metres long. Lines 0, 20N, 60N, and 75N were sampled at 20 metre intervals, line 40N was sampled every five metres. The lone

north/south line was placed at 100 metres east and was sampled in five metre increments from 0 metres north to 85 metres north. Lines 100E and 40N were sampled more finely in order to observe the effect of very short spacing variations in conductivity. East/west oriented barbed wire fences at about 5 metres south and 85 metres north, and a north/south fence at 40 metres west were the only significant cultural features noted in the area. The grid was constructed using a chain and pin flags and oriented to parallel the fence lines. Line locations are shown in figures 4.5, 4.6 and 4.7.

EM31 data were also collected at the nearby gravel pits. In both cases, 100 m of EM31 data were acquired with 5 metre station spacings on a bench in the pit where the overlying tills had been removed. Single point readings were obtained adjacent to the pits over undisturbed material.

### 4.3.3  Data Processing and Interpretation

Processing applied to these data consists largely of removing obvious noise bursts and the iterative process of choosing appropriate mapping parameters. The data were carefully monitored in the field to anticipate the presence of cultural features which might produce signal that could overprint the earth conductivity response. By rotating the EM31 through 90° about a vertical axis at a station and observing variations in the conductivity reading, the presence of nearby, linear, highly conductive objects may be observed. If the apparent conductivity value changes dramatically for the two positions of the instrument at one survey location the change is attributed to variations in coupling, and the likelihood is that nearby anomalies are caused by linear conductive features such as fences or pipelines.

It is possible to forward model the data obtained with these instruments so that a more quantitative evaluation of conductivity structure can be obtained. Geonics provides simple expressions to calculate instrument response given a layered earth model (McNeill, 1980*b*). These expressions have been used to model the response of the EM34-3 vertical dipole measurements (Figure 4.4). The approach is to firstly, assume a two-layer earth model then secondly, plot the measured data against a theoretically derived curve and lastly, to perturb the model parameters until a close match is made between the

theoretical curve and the field data. There are only three data points to use in electronic curve matching, so it is not reasonable to assume more complexity to the earth than that it be two-layered.

This process was applied to field data throughout the farm grid. The modelling was performed both without external constraints (assuming two layers of unknown thickness) and constraining the first layer thickness (assuming a two-layered earth whose upper layer was 12 metres thick). This latter value is obtained from the seismic refraction and VES interpretation. For the unconstrained models, first layer thickness estimates vary from 16 to 18 metres at about 20 mS/m conductivity, second layer conductivity of about 9 mS/m. The models restricted to 12 m thickness yield upper layer conductivity of about 20 mS/m and lower of about 10 mS/m.

Conductivity maps are provided as Figures 4.5-4.7. These are simply presented as contours of the apparent conductivity values for each instrument mode produced using software designed by Geosoft Inc. The contour interval for all maps is 2 mS/m. The contouring uses minimum curvature techniques for gridding, and allows for the introduction of a tension parameter to vary the result. The algorithm produces a surface which approximates a thin flexible sheet passing through the data points. The tension parameter varies the tension of this sheet (Smith and Wessel, 1990). Testing suggested that gridding using no tension provided the optimum result (i.e. the result which most closely matched hand contouring).

Figure 4.5 includes maps of all EM31 instrument modes obtained, Figure 4.6 includes maps of EM34-3 vertical dipole measurements, and Figure 4.7 includes maps of EM34-3 horizontal dipole measurements. The maps show a number of anomalies, all of which are coded by letter and shading. The homogeneity of the conductivity response appears to increase from EM31 to EM34-3 vertical dipole to EM34-3 horizontal readings. The EM31 response is legitimately more complex than the others - it samples a much smaller portion of the earth and should be able to better resolve short wavelength changes in conductivity. The EM34-3 vertical dipole response is strongly perturbed by a cultural feature (barbed wire fence) at about 5 m south. Without this effect, it is probably closer

to the EM34-3 horizontal dipole maps in response homogeneity. The anomalies identified on the maps are listed in Table 4.4 and characterised by the depth of the anomaly source and the sense of the anomaly.
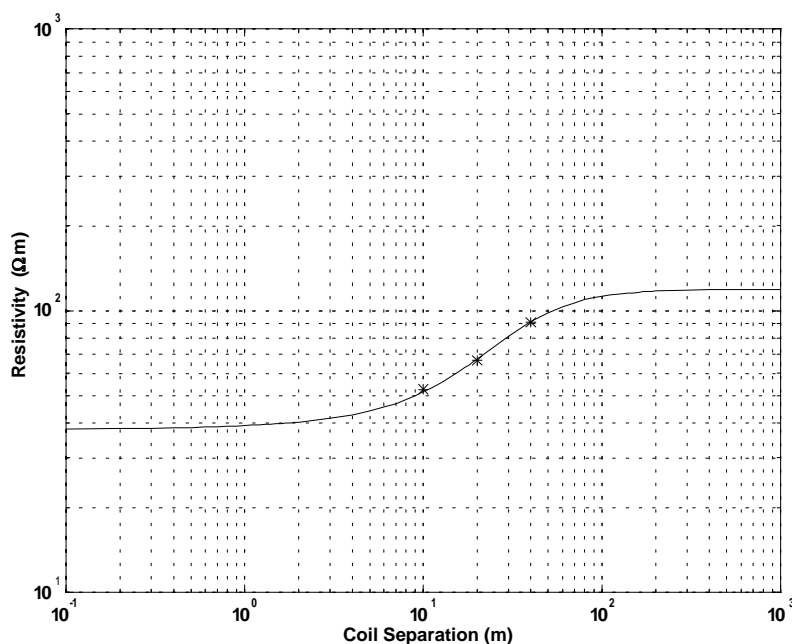


**Figure 4.4**    Forward model for EM34-3 vertical dipole data. Three apparent conductivity values for readings at 10, 20, and 40 metre coil spacings are fitted to a modelled two-layered curve. Measured conductivities (resistivities) are 19 (53), 15 (67) and 11 (91) mS/m (Ωm) for each spacing respectively.

Anomalies which repeat from one map to the next in depth probably arise from shallow variations in conductivity, while those which only appear at increasing depths are interpreted to be due to deeper sources. Local high-conductivity pockets on the shallow data maps (Figure 4.5) likely result from variations in thickness of clay rich till. Local low conductivity areas generally result from increased thickness of gravel or laterally limited zones of more coarse grained material lying within the tills.
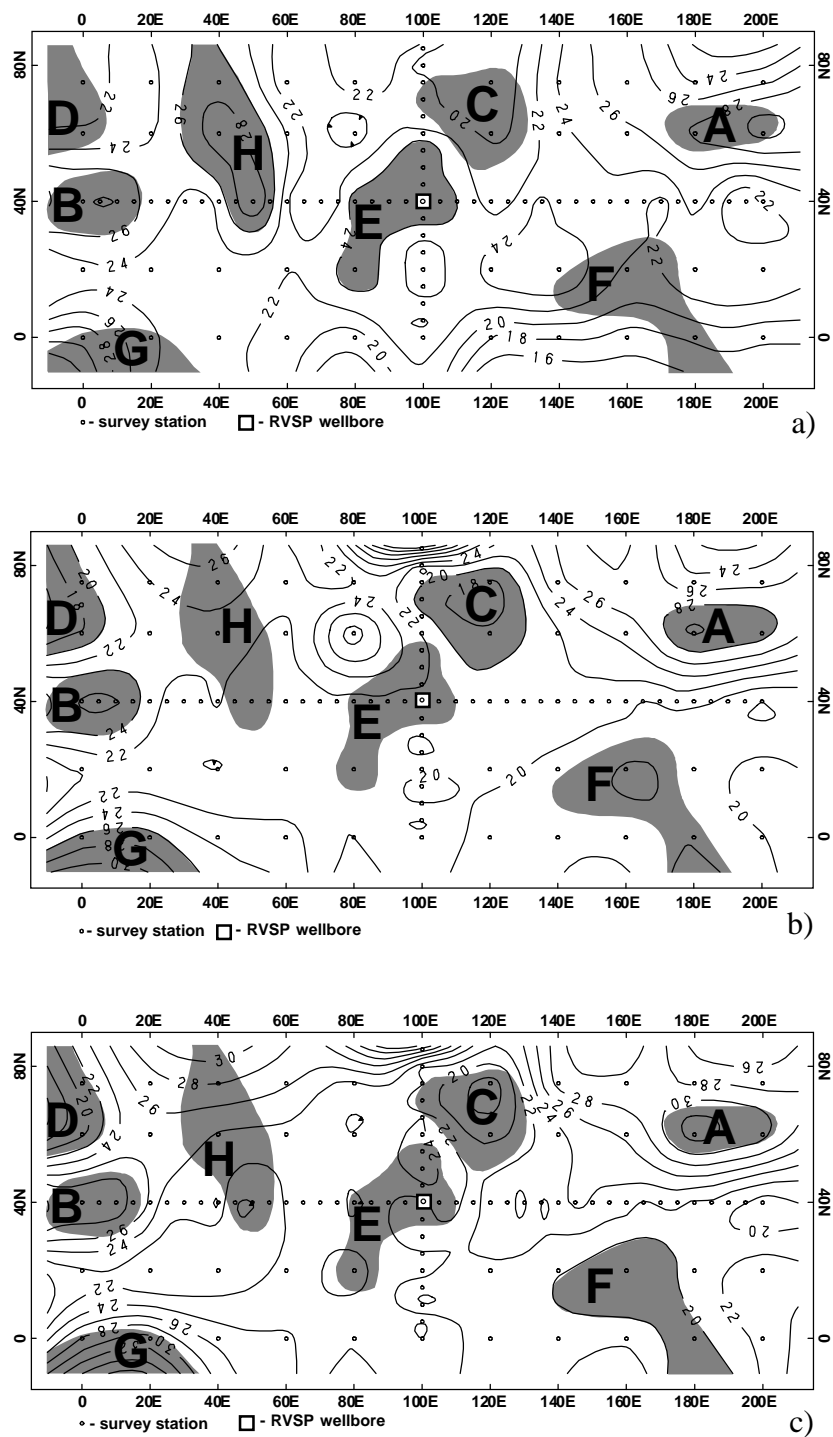
**Figure 4.5** Apparent conductivity maps - EM31 instrument. a) Hg measurement mode (horizontal dipoles, 0 m elevation), b) Vz measurement mode (vertical dipoles, 1 m elevation), c) Vg measurement mode (vertical dipoles, 0 m elevation).
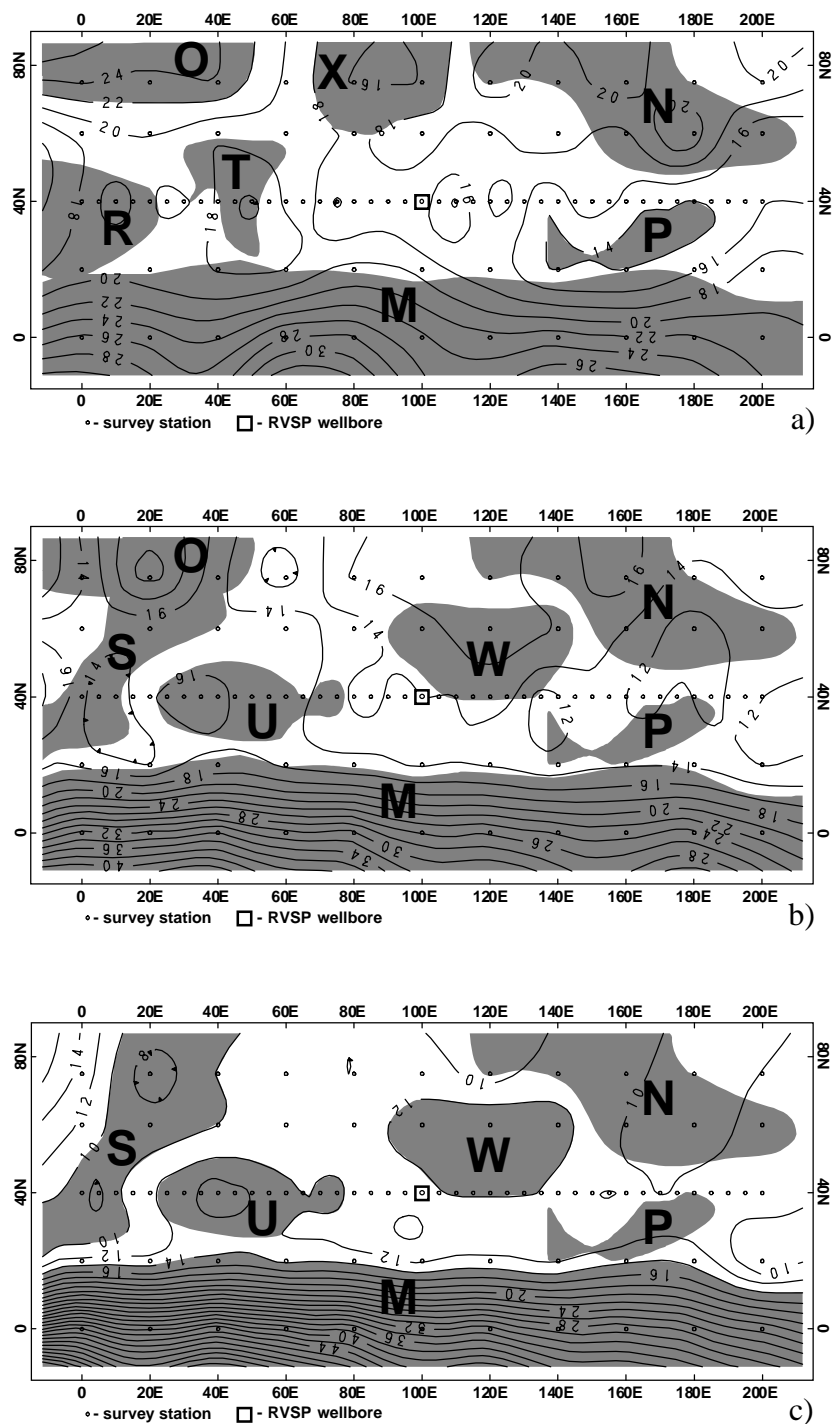
**Figure 4.6**  Apparent conductivity maps - EM34-3 instrument.  a) 10V measurement mode (10 m vertical dipoles), b) 20V measurement mode (20 m vertical dipoles), c) 40V measurement mode (40 m vertical dipoles).
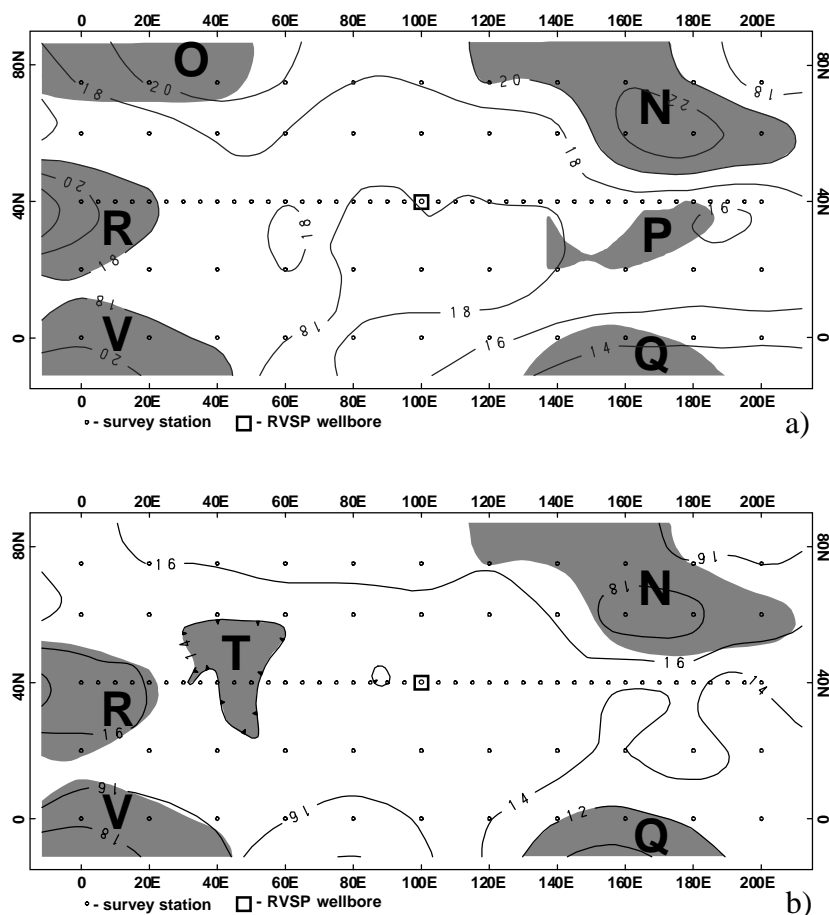
**Figure 4.7** Apparent conductivity maps - EM34-3 instrument. a) 20H measurement mode (20 m horizontal dipoles), b) 40H measurement mode (40 m horizontal dipoles).

The anomaly designated as **M** is the largest and strongest on any of the maps. It is only apparent on the EM34-3 vertical dipole maps (Figure 4.6), and results from a barbed wire fence at 5 metres south. The horizontal dipole does not couple well with the fence and so the fence effect is not apparent for measurements using this orientation (Figure 4.7). The relative response at each depth is not the same for horizontal as for vertically oriented dipoles. Horizontal dipoles are biased more toward identification of shallower features and vertical dipole measurements to mid-depth features (McNeill, 1980*b*). The result is that differences are evident between the EM34-3 10V and 20H and the EM34-3

20V and 40H maps (Figures 4.6 and 4.7) even though each of these mode pairs share the same effective depth of exploration.

**Table 4.4** Apparent Conductivity Anomalies

| Anomaly | Conductivity Increase/Decrease | Source Depth (d) |
|:---:|:---:|:---:|
| A | Strong Increase | $d < 6m$ ($> 3m$?) |
| B | Moderate Increase | $d < 6m$ |
| C | Moderate Decrease | $d < 6m$ |
| D | Moderate Decrease | $d < 6m$ ($>3m$?) |
| E | Slight Increase | $d < 3m$ |
| F | Slight Decrease | $3m < d > 6m$ |
| G | Strong Increase | $d < 6m$ |
| H | Moderate Increase | $d < 3m$ |
| M | Very Strong Increase | $d < 0m$ |
| N | Moderate Increase | $d < 30m$ |
| O | Strong Increase | $d < 30m$ |
| P | Moderate Decrease | $d < 15m$ ($d < 30m$?) |
| Q | Moderate Decrease | $d < 30m$ |
| R | Moderate Increase | $d < 30m$ |
| S | Moderate Decrease | $d > 30m$ |
| T | Slight Decrease | $d < 30m$ |
| U | Moderate Increase | $d > 30m$ |
| V | Moderate Increase | $d < 30m$ |
| W | Slight Increase | $d < 30m$ |
| X | Slight Decrease | $d < 15m$ |

The nearby gravel pits confirm the low conductivity nature of the gravels (Figure 4.8). EM31 data collected there are compared with data collected at the farm site. The conductivity measured at the pit sites (where the till has been stripped) averages to about 2.1 mS/m (480 $\Omega$m resistivity). Adjacent to the pits, where the till is still in place, conductivity was measured at 33.3 mS/m (Lafarge Pit) and 38.6 mS/m (Standard General Pit) for the Vg orientation.
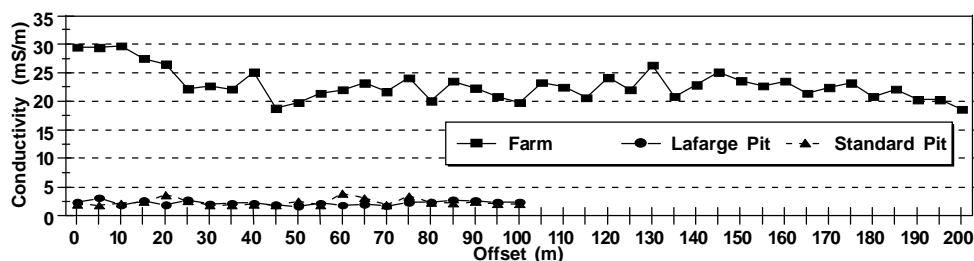


**Figure 4.8** EM31(Vg) apparent ground conductivity profiles. The pit sites are locations of exposed gravel - the farm site is undisturbed and covered by 12 metres of till.

## 4.4 Comparison of Conductivity/Resistivity Investigations

The materials investigated by VES and FEM techniques at the three sites are lithologically similar. Their electrical character is also similar. No direct comparison can be made between the values measured by these two methods unless the investigated feature approximates a half-space - FEM measurements will otherwise be influenced to a large extent by the over- or under-lying layers. The apparent conductivity measured using FEM tools does approximate that of a half-space for the shallow reading modes in the tills and in the gravel pits where the till has been removed. Table 4.5 provides a ready comparison of the conductivity (and resistivity) values obtained by these two methods. It is clear that the values of conductivity (resistivity) obtained via both methods are similar for similar examined lithologies. This lends credence to the VES interpretation as we are confident of the resistivity values obtained using FEM over a half space. The close comparison in resistivity suggests that the VES model obtained by inversion yields a good estimate of the true earth resistivity.

**Table 4.5**  Comparison of Electrical Conductivity (Resistivity) Values from the Two Methods

|  | Farm VES mS/m ($\Omega$m) | Farm FEM mS/m ($\Omega$m) | Lafarge FEM mS/m ($\Omega$m) | Standard General FEM mS/m ($\Omega$m) |
|---|---|---|---|---|
| Till | 25.8 (38.8) | 23.3 (42.9) | 24.9 (40.2) | 34.5 (29.0) |
| Gravel | 2.0 (503) | N/A | 1.9 (529) | 2.0 (529) |

The FEM method does not lend itself readily to quantitative estimations of depth extent for electrostratigraphic units.  The attempt made using the farm EM34-3 vertical dipole data to produce such an estimation yields a two-layer model whose upper layer is 12 metres thick.  The conductivities derived are 20 mS/m (upper layer) and 10 mS/m (lower layer).  The depth estimate is in good agreement with the VES derived upper layer depth of 12.5 metres.  The conductivity values do not agree.  The VES values are 25.8 mS/m (upper layer) and 2.0 mS/m (lower layer).

## 4.5 Ground Penetrating Radar Studies

### 4.5.1 Introduction

The GPR technique consists of directing a pulsed input of high-frequency electromagnetic energy into the earth and recording the returning energy reflected and refracted from boundaries across which there is a contrast in dielectric constant.  The GPR pulse consists of a band of frequencies about a peak value which falls in the range 10-1000 MHz.  The bandwidth produced is normally approximately equal to the peak frequency value (i.e. a 50 MHz peak antenna produces signal with a bandwidth of 50 MHz).  Reflection, refraction and depth of penetration are governed by the choice of central frequency, bandwidth, and the electrical properties of the geological materials being investigated, most notably dielectric constant ($\kappa$), conductivity ($\sigma$), and attenuation ($\alpha$) (Davis and Annan, 1989).

GPR data are most often recorded at fixed locations and plotted as a time series, usually referencing the location to a midpoint between the transmitting and receiving antennae (profiling). By juxtaposing a number of evenly spaced traces, a cross section of the reflection dielectric structure of the earth is formed. This image can be interpreted to infer geological structure, presence of contaminants within the earth, cultural features, voids, or other electrical contrasts (Daniels, 1989). Often a common midpoint (CMP) dataset is obtained at the same site, which allows the interpreter to compute the radar wave velocity within the earth to assist in time-depth conversion.

At least two features should be identifiable on any two antenna (bistatic) GPR profile (Figure 4.9). The first of these, the airwave arrival, travels through the air at 0.3 m/ns and the second, the groundwave arrival, travels a path just below the air/ground interface at a velocity depending largely on the dielectric constant of the near-surface material. For small, fixed offset surveys, the instant of the airwave arrival is taken as the zero time for the section and the groundwave as the zero depth (Annan and Cosway, 1992). Other events observed on the section may be reflections from within (and possibly above) the earth, diffractions, and noise.
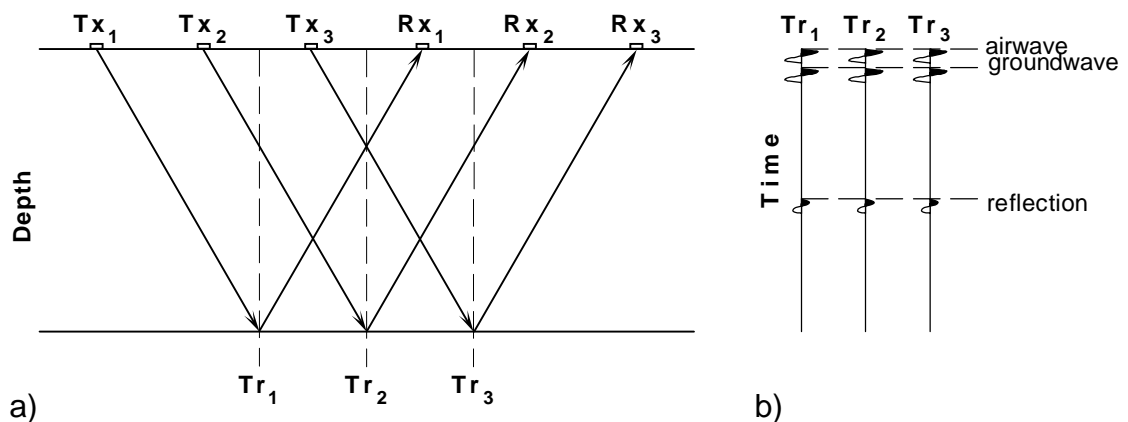


**Figure 4.9** GPR profiling geometry for bistatic antenna configuration. a) depth section and b) time section. $Tx_n$ is the transmitter antenna location, $Rx_n$ is the corresponding receiver antenna location and $Tr_n$ is the reflection location.

For a CMP image (Figure 4.10), the transmitter and receiver are stepped out by some fixed increment between each trace. The groundwave and airwave arrivals then form straight lines on a $t$-$x$ plot from which their velocity may be calculated directly. If reflections are strong enough to be evident on the longer offset traces, a velocity/depth profile may be obtained by computing the rms velocities ($V_{rms}$) for each observed reflection based on the relationship:

$$t^2 = t_0^2 + x^2/V_{rms}^2 \, ,$$

where $t$ is the arrival time on any given trace, $x$ is the offset of that trace, and $t_0$ is the zero-offset reflection arrival time.
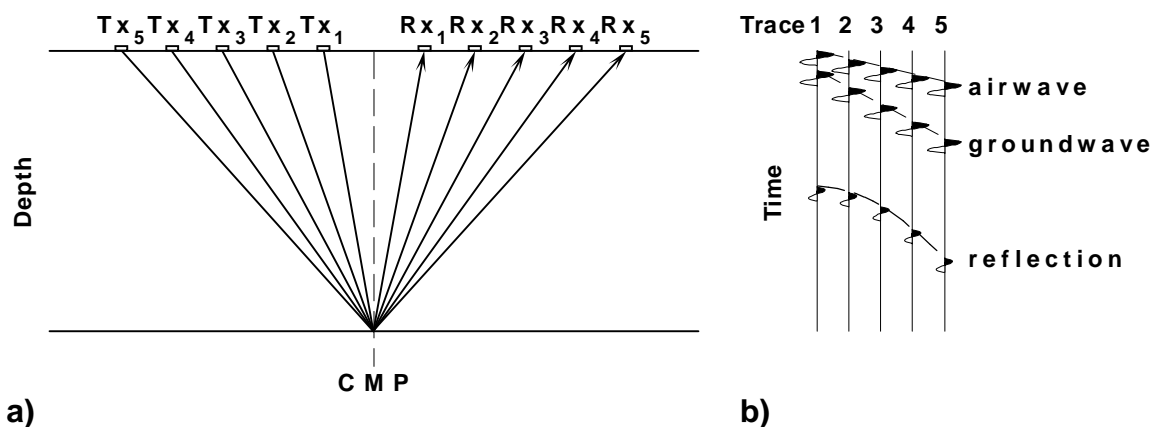


**Figure 4.10**   GPR CMP geometry for bistatic antenna configuration.  a) depth section and b) time section.  $Tx_n$ is the transmitter antenna location and $Rx_n$ is the corresponding receiver antenna location.

There are a number of limitations to the applicability of the GPR method. Regions of higher ground conductivity (>10 mS/m) restrict depth of penetration to the order of metres - signal attenuation is directly related to conductivity.  Typical investigable depths in lower conductivity areas are closer to 10-20 metres.  In very resistive materials (e.g. granite), conductivity can be as low as  0.01-1 mS/m, resulting in penetration as great as 110 m (Kalantzis et al., 1994).  Attenuation is not solely related to

conductivity, frequency is also a factor. It is generally the case that higher frequencies provide greater potential resolution, but are attenuated more rapidly, leading to decreased depth of penetration of the GPR signal (Davis and Annan, 1989; Jol, 1995). Antenna frequency is chosen as the best compromise between these two factors.

### 4.5.2 Data Acquisition

GPR data were acquired at three distinct locations: the RVSP site, the Lafarge gravel pit, and the Standard General gravel pit. The operators of the gravel pits strip all of the clay-rich till before extracting aggregate materials, so surveys at those two sites allowed for an investigation of the gravel material without its attenuative overburden. The Lafarge pit is about 1.7 km northeast, and the Standard General pit is about 3.4 km southeast of the RVSP site. The RVSP site surveys were performed on April 14, 1994. They consist of a north/south and an east/west profile, both centred over the RVSP wellbore. The gravel pit surveys consist of north/south profiles and CMP sections at each site and were performed on April 21, 1994. The gravel benches were too narrow to allow east/west profiles. All data were acquired using a Sensors & Software Inc. pulseEKKO IV GPR system owned by the University of Calgary's Department of Geology & Geophysics. The acquisition parameters for the profiles are listed in Table 4.6.

**Table 4.6**  GPR Acquisition Parameters

| | |
|---|---|
| Frequency | 50 MHz |
| Antenna Separation | 1.0 m |
| Station Spacing | 1.0 m |
| Sampling Interval | 800 ps |
| Number of Stacks | 64 or 128 |
| Pulser Voltage | 400 V |

GPR data were acquired by a two-person crew. One crew member (crew 1) attended to the movement of the antennae, while the other (collector) controlled trace collection via software. If antenna separations of 2 m or more are used, a third crew

member (crew 2) is a useful addition - this allows for more rapid data acquisition as the antennae can be moved simultaneously.

The method employed was to lay out a 100-metre-long, 1 metre graduated nylon chain on the ground and to use this as both a means of maintaining constant antenna separation and of locating survey stations.  The chain is preferred over a fibreglass tape measure as the latter can be greatly affected by even light winds.  The collector carried both the GPR console and a laptop computer which was used for both real-time data observation and file storage.  The console and computer (and hence, the collector) were connected to the antennae by 20 m long fibre optic cables to remove the influence of the broadcast EM fields as far as possible.  The crew was notified by an audible tone when a trace had been collected; they then advanced the antennae to the next station.

For the CMP sections, the same field equipment is used.  The first trace was obtained with the antennae spaced 1 metre apart at the 49.5 and 50.5 metre mark of the tape.  After the first trace was acquired, the antennae were each moved 0.5 metres outward and another trace was obtained.  This procedure was repeated until the received signal level was lost in background noise.  The CMP gathers obtained by this procedure are shown in Figure 4.11. The CMP gather for the Lafarge pit was acquired with a pair of 100 MHz antennae, the Standard General with 50 MHz; both used an 800 ps sampling interval.  Airwave, groundwave and reflection events are evident on both.  Reflection events are identifiable to just over 200 ns time at near offsets, which equates to about 12 metres depth.  Velocity values shown on the figures are layer velocities for the airwave and groundwave and interval velocities for the reflection events.

The pulseEKKO software allows the collector to apply a minimum amount of processing to the data as they are being acquired in order to gauge the effectiveness of the acquisition parameters and to apply real-time quality control.  Our procedure was to estimate the appropriate parameters from assumptions pertinent to the field area ahead of time, and to adjust them as necessary when in the field.  These adjustments had mostly to do with the gain applied, sample interval and the trace length.
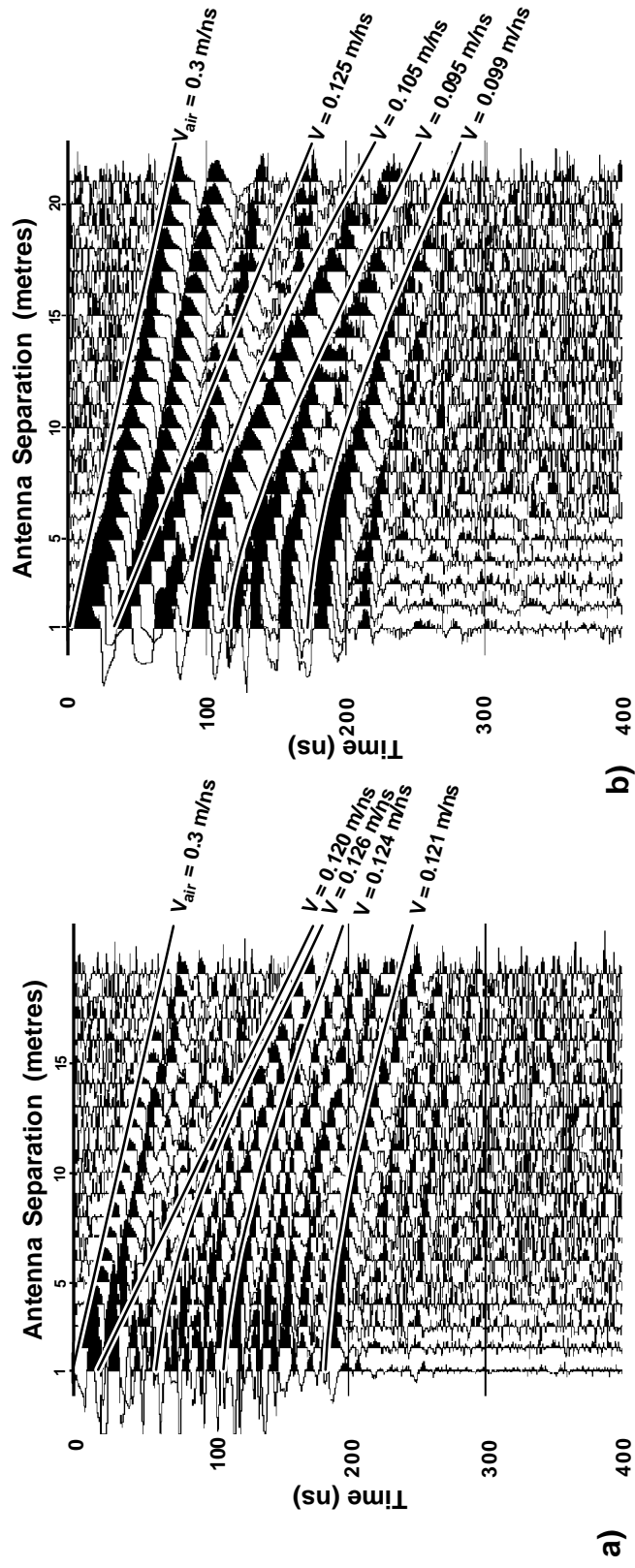
**Figure 4.11** CMP soundings for gravel pit sites. a) Lafarge Gravel Pit - 100 MHz antennae, b) Standard General Gravel Pit - 50 MHz antennae. SSC applied, 10 ns AGC.

### 4.5.3 Data Processing

Sensors & Software Inc. provide software with their GPR hardware to control data acquisition and to effect a minimal processing stream. Some of these processes are unique to GPR signal analysis and are always applied to the data. Most of the additional processing steps have been borrowed from seismic reflection analysis. The flow of processing steps used for the profiles in this study is shown in Table 4.7. The result of the most effective of these processes are illustrated in Figure 4.12.

Signal saturation correction (SSC) is required to remove both a slowly decaying low frequency wow and DC shift which are artifacts produced during data acquisition. They are removed by applying a specially designed (essentially) low-cut filter in pulseEKKO. The filter is automatically applied to all trace data displayed or printed from within pulseEKKO, but must be explicitly applied before exporting the data to a non-native format such as SEG-Y. This conversion was required in order to undertake further processing using ProMAX seismic data processing software.

**Table 4.7**   GPR Processing Flow

| Signal Saturation Correction |
|:---:|
| SEGY Conversion |
| Airwave Flattening |
| NMO Correction |
| Bandpass Filter |
| AGC (restricted) |
| $f\text{-}x$ Deconvolution |

**Figure 4.12**   GPR sections obtained at the Lafarge gravel pit shown at various stages in the processing stream.  a) imported from pulseEKKO format to SEGY format and displayed with 100 ns agc.  b) flattening, bandpass filter, restricted agc, and NMO corrections.  c) full processing, including *f-x* deconvolution.

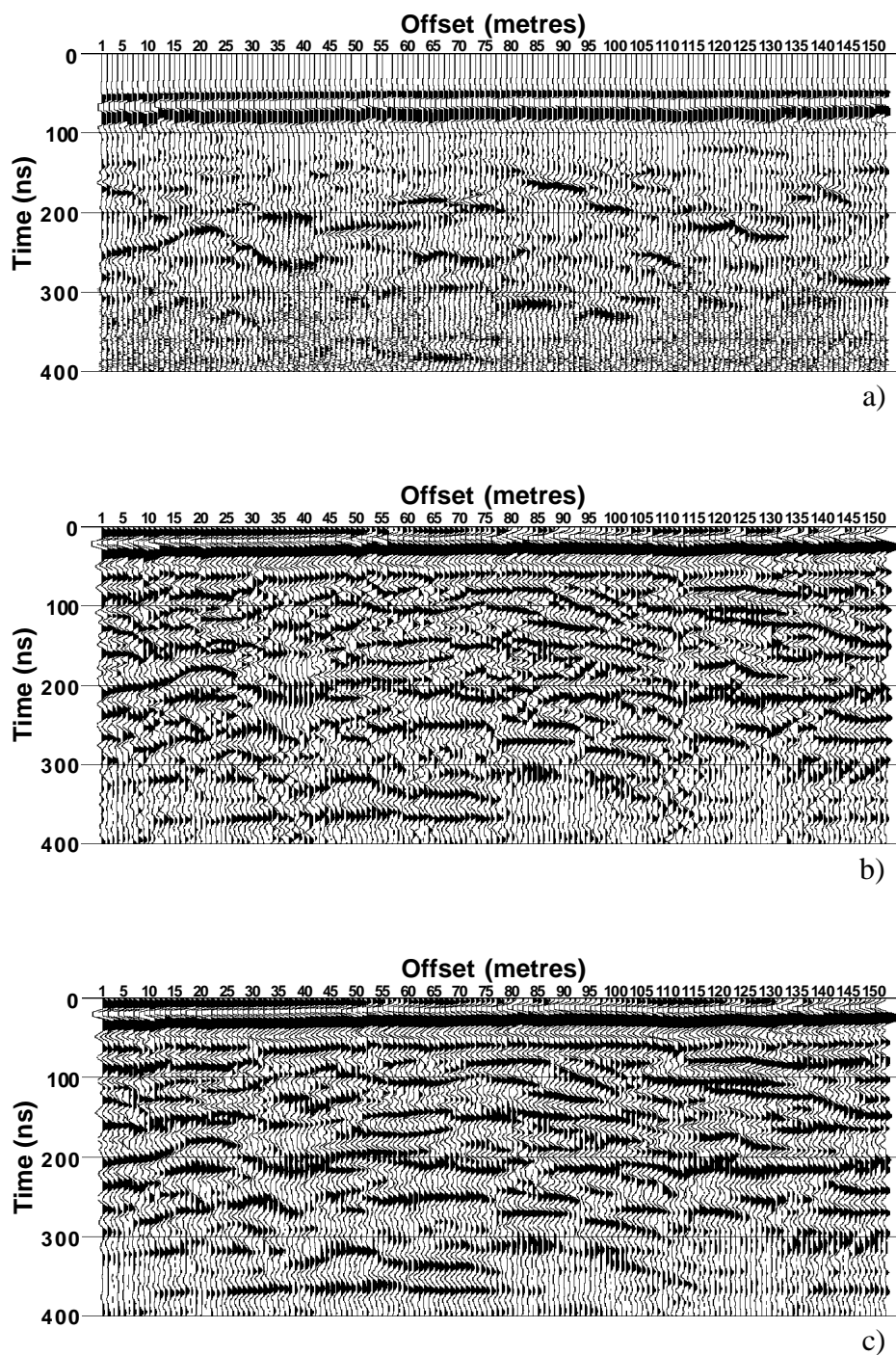If data are acquired before the machine has had an opportunity to reach a stable operating temperature or if the ambient temperature changes dramatically while acquiring a profile, the time of the airwave arrival will vary across the profile. Radar trace acquisition begins before the transmitting antenna begins broadcasting in order to estimate noise. The lag time between trace acquisition and source excitation will vary with the operating temperature of the instrument. Time-zero shifts also occur from slight inaccuracies in antenna placement. For large variations in time-zero, the automatic correction routines in pulseEKKO fail, and a trace by trace adjustment is necessary. Once the data are transferred to the seismic processing software, the time-zero shift must be explicitly applied as a bulk static shift (it is automatically applied before viewing or plotting any trace data in the radar software). This value is stored in the file headers for all GPR sections.

Some of the processes which may be applied to these data require that traces be in zero-offset two-way traveltime. Normal moveout (NMO) corrections, based on groundwave and rms reflection velocity, achieve this goal. This correction is necessary to allow for accurate depth conversions and has its greatest effect on the shallowest reflectors.

Bandpass filtering assists in the removal of (mostly) high frequency noise. The filter parameters used here were based on 10 MHz (corner frequency) wide filter panels that show significant reflection information at lower frequencies, essentially disappearing above 70 MHz (for the 50 MHz antennae). The Ormsby filter used was 5/15-70/110 MHz.

A variety of gain schemes were investigated and automatic gain control (AGC) was chosen. By restricting the applied gain to a maximum of 10 times median gain, a very short AGC window (20 ns) boosted all reflection amplitudes so that they were easily identifiable. This also left low amplitude noise (especially at later times) relatively untouched, and allowed the use of such a small window. Both AGC and bandpass filtering were applied over windowed portions of the sections. Time gates were constructed that identified the highest true amplitude first arrivals and the later reflection

information.  These two zones were treated separately so that each was of approximately equal average absolute amplitude after the frequency filter and gain processes.  This made the reflection events appear stronger than was the case when the two zones were treated as a single unit.

The final process applied was *f-x* deconvolution.  Its application was primarily an attempt to enhance spatially coherent information in the sections.  This provided a substantial improvement in reflection coherency, greatly enhancing correlatability and interpretability.  Migration attempts were unsuccessful, largely because the data were acquired at a broad station spacing.  The Nyquist sampling interval ($\Delta_n$) for peak antenna frequency  and the local earth parameters is 1.2 m. For the highest frequencies present in the data $\Delta_n$ is 0.8 m.  This is perilously close to the acquisition station spacing, suggesting that these data may be spatially aliassed for any significant dips in reflectors.

### 4.5.4 Data Interpretation

All sections have been subjected to the same processing sequence.  It is clear that the RVSP site section (Fig. 4.13) provides limited information about the earth's local dielectric structure.  No reflections are obvious on section 4.13, although a feature at about 4 metres depth may be interpreted as an internal till reflection.  The feature at about 7 metres apparent depth is most likely a multiple of the groundwave or a combined airwave/groundwave multiple.  These multiples occur as a result of airwave reflections between the antennae.

Indications from other methods (seismic refraction, VES) are that the tills are about 12.5 metres thick at the RVSP site and that they average close to 26 mS/m in electrical conductivity.  Using Annan and Cosway's (1992) rule of thumb electrical conductivity based estimation suggests that for a conductivity of 26 mS/m, the maximum depth of investigation for GPR is 1.5 metres.  A more formal approach (the radar range equation - RRE) which accounts for signal loss due to system, propagation and target factors is presented by Annan and Davis (1977) and by Annan and Chua (1992).  Using the RRE and assuming a two-layered earth with transmission host dielectric constant of

10, a reflection target dielectric constant of $20^{4.2}$ and 50 MHz antenna frequency, an interface at 4.0 metres depth would only contribute recognisable signal after $6.7 \times 10^5$ traces had been stacked. This is an impractically large number, the data collected at the RVSP site were stacked 128 times. The event at about 160 ns time is then (based on both rule of thumb and RRE criteria), unlikely to be a reflection from near the limit of investigation.
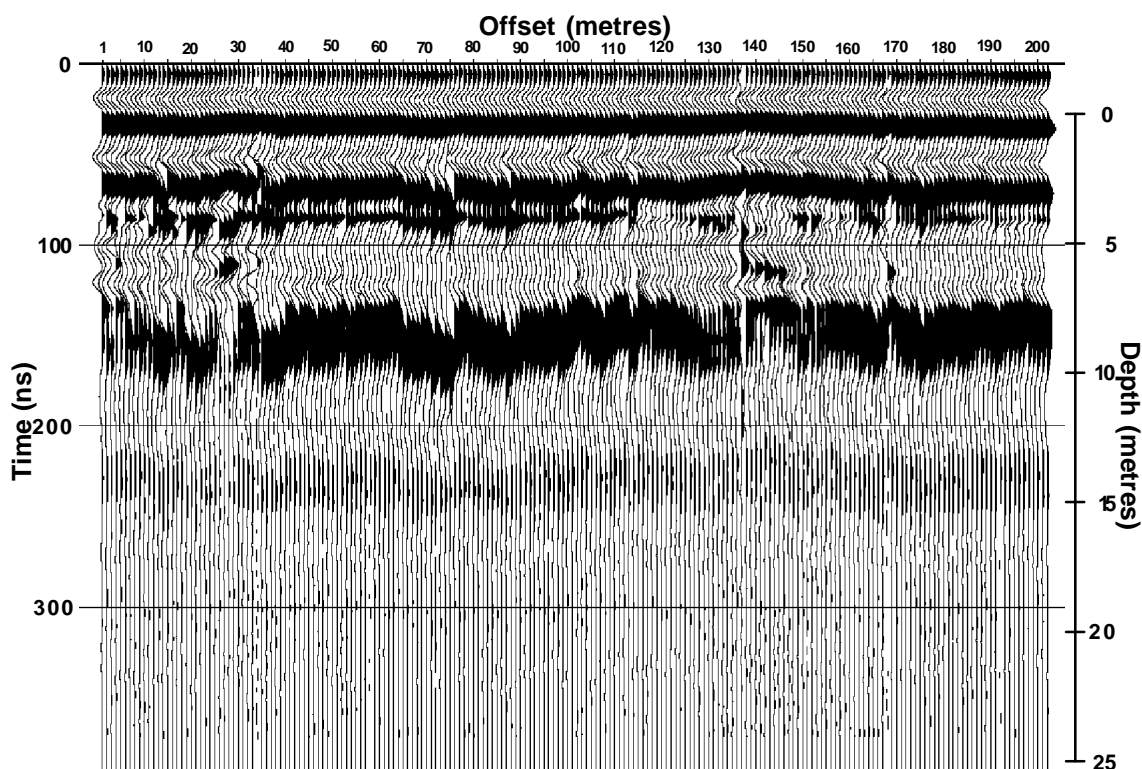


**Figure 4.13** RVSP site GPR section over highly attenuative clay-rich till. 50 MHz antennae. Fully processed section. No *f-x* deconvolution applied.

Figures 4.14 a) and 4.15 a) are the processed sections for the Standard General and Lafarge gravel pits respectively. At these locations, no high conductivity till remains

---

[4.2] This assumption is a reasonable one and is based on the lithology at the site. It considers the reflector to be a wet clay-rich till underlying a dry clay-rich till.

to limit signal penetration. Both profiles contain reflection events from interfaces greater than 15 metres depth; the Lafarge pit section from about 18.5 metres and the Standard General section from about 16 metres. These sections point out a difficulty with GPR data - the shallowest portion of the earth (less than about 4 metres depth) is not investigated. Whatever reflection events may exist within this zone are swamped by the overwhelmingly high amplitude airwave and groundwave arrivals. Considerations of the resolution/depth of penetration trade off are usually focussed on the determination of maximum depth of penetration. These sections suggest that, if one is interested in both the most shallow portion of the earth as well as deeper zones, multi-frequency studies are necessary.

The character of the reflection tracings reveals the depositional fabric of the aggregate materials (Figures 4.14 b and 4.15 b). These figures were prepared by tracing continuous, coherent reflection events on the GPR sections and are essentially overlays of those tracings on the section time and depth axes.

The braid plain stream system which deposited the gravel materials here propagated east out of the mountain front. Both gravel pit sections are oriented north/south. Both show the complex inner structure of the braid plain regime, with average bed thickness of $1.6 \pm 0.3$ (Lafarge) and $1.7 \pm 0.2$ metres (Standard General) respectively. The Lafarge pit section is suggestive of more cross-cutting bed relationships, the Standard General section appears more tabular in nature. Either the energy regimes differed for deposition at the two different sites (Lafarge higher energy, Standard General lower), or the sections differ in their orientation with respect to ancient flow direction.
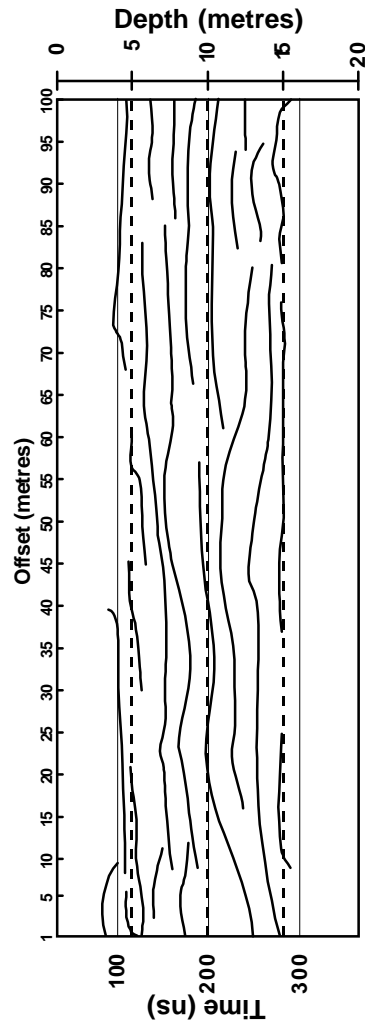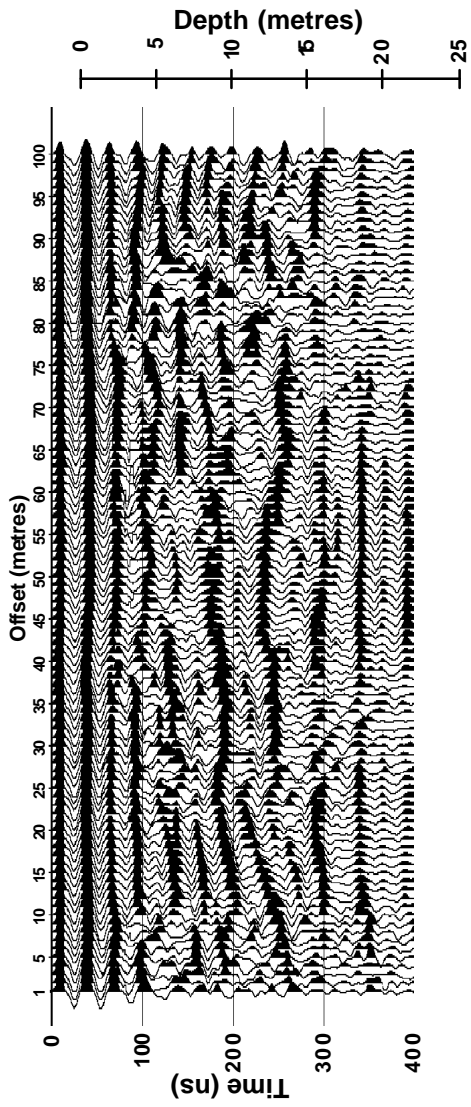
**Figure 4.14** GPR and interpretation sections from the Standard General Gravel Pit. a) 50 MHz antennae, fully processed section, b) reflection tracings of high amplitude events.
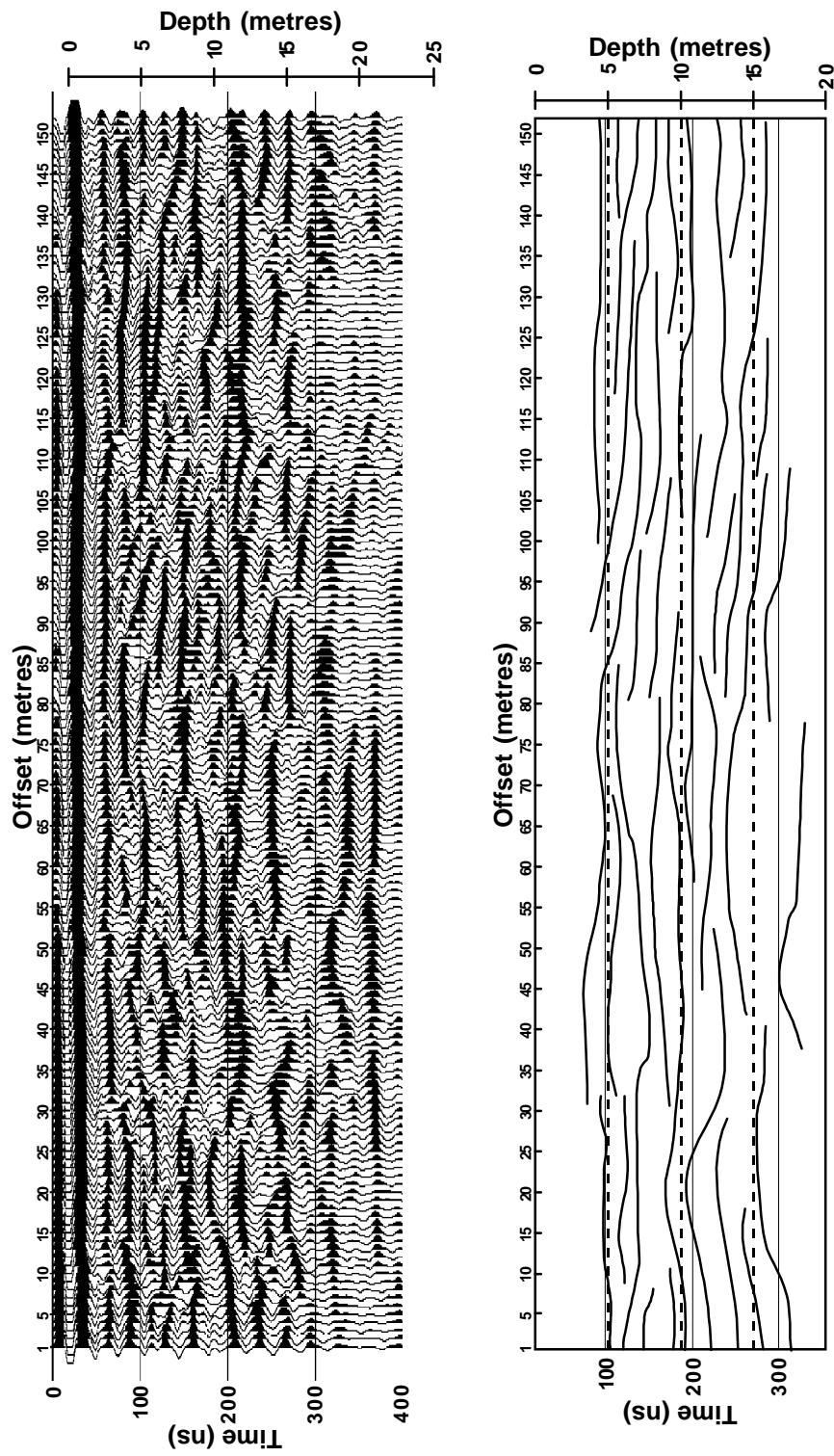
**Figure 4.15** GPR and interpretation sections from the Lafarge Gravel Pit. a) 50 MHz antennae, fully processed section, b) reflection tracings of high amplitude events.

**Chapter 5. Conclusions**

Of the five geophysical techniques applied in this series of investigations, some were individually successful, some were made more successful in concert with the result of other methods, and some were of limited value at specific sites. More background information regarding site geology would have been invaluable in planning this series of investigations.

RVSP results were coloured by deficiencies in data acquisition. Traveltime inversion showed a relatively high third layer velocity that may be attributed to source movement. A more reliably located source would have done much to improve the quality of the traveltime inversion and may have eliminated the need for the second refraction survey. A single downhole explosive source suspended on a wireline and reloaded for each shot should be an improvement over the prepared string of sources. (A perforating gun might be a suitable source.) This would provide more trustworthy shot depth estimation at the expense of greater acquisition time. At the very least, it would indicate the condition of the hole between shots. Higher frequency sampling would have been useful to retrieve higher frequency data. With a Nyquist frequency of 250 Hz, the fine resolution in time necessary to effect complete wavefield separation was not available. Consequently a brute stack approach to RET generation had to be employed. In such a shallow survey as this one, physically small offsets in receiver location are large relative to shot depth. Complications arising from wide reflection angles appear very quickly. Finally, when a borehole is drilled for the purpose of an RVSP, it is necessary to glean whatever geological information is available during the drilling operations. A lithological log for the RVSP hole would have been very useful in confirming the interpretations of all the geophysical techniques employed here. Even with the acquisition difficulties it was still possible to produce an interpretable RET for both *P*-waves and converted *S*-waves which provides seismic information from below the bottom of the borehole.

The gross electrical character of the earth was revealed by vertical electrical sounding. The profile resulting from this technique is attributed to a single point on the earth (one dimensional model) even though progressively deeper investigating dipoles

require progressively wider spaced electrodes. This suggests that deeper features evident on such a survey may be more laterally extensive than shallow features. The measured conductivity for the profile derived from VES at the farm site is in good agreement with data from fixed frequency electromagnetic data, providing increased confidence in the VES result.

The FEM data suites do not provide a reliably quantifiable image of the local electrical conductivity structure of the earth. They do, however, provide a good indication of the lateral distribution of electrical conductivity over qualified depth intervals (the effective depths of investigation). They also confirm the conductivity (resistivity) values derived from the VES. By mapping the FEM data, the lateral homogeneity/heterogeneity of the earth is revealed. This can be useful information in assessing the validity of the VES data. In this study, the indication is that the thinner upper conductivity layering evident on the VES is attributable to local lithological variations.

Ground penetrating radar profiling provided the most detailed image of the earth at any of the sites investigated, but was restricted in its use in the general case. The limited range of conductivities that allow the successful application of GPR are a significant problem in areas with overburden of high conductivity such as clay-rich glacial till. In those locations where the electrical conductivity of the earth is low enough to make GPR investigations practically useful, the quality of the image derived is good enough to observe very small scale variations in lithology from which one can infer details of depositional fabric. If a GPR investigation is to identify features in the very shallow (< 5 m) zone as well as deeper features, the survey must use multiple antennae with several different peak frequencies.

Refraction profiling produced an image of the gross acoustic character of the near-surface at the farm site. The level of detail achieved there depended heavily on the very dense shot interval and receiver spacing. Two different refraction surveys were undertaken, primarily because the first (which had exclusively used a $P$-wave source) did not contain enough long-offset information to apply a rigorous refraction interpretation

scheme and was not interpretable for *S*-wave arrivals. The results for the two different reciprocal spread interpretation schemes applied to the second data set were very closely matched. The GRM scheme is preferred if significant refractor structure is evident, if a lateral velocity variation is suspected, if a thin (unresolved) layer is suspected, or if a velocity inversion is likely. In fact, the criteria for identifying appropriate interpretation parameters (XY spacing) for the GRM demands that some structural variation occur along the profile. The plus/minus is a simpler scheme to implement and does not require geological structure for its successful application.

Those methods which provide interpretable information regarding the local geology reveal a layer of clay-rich till material of about 12 metres thickness astride a thick deposit of gravel. The refraction data suggest the existence of a layer of increased water saturation from about 3.5 to 12 metres depth. Desiccation of the shallowest portion of the earth (likely resulting from climactic conditions) is suspected as the cause. DC electrical investigations and traveltime information from the RVSP supports this observation.

# References

Annan, A.P., and Davis, J.L., 1977, Radar range analysis for geological materials: Report of Activities, Part B: Geological Survey of Canada, Paper 77-1B, 117-124.

Annan, A.P., and Chua, L.T., 1992, Ground penetrating radar performance predictions, in Pilon, J. Ed., Ground penetrating radar, Geological Survey of Canada, Paper 90-4, 5-13.

Annan, A.P., and Cosway, S.W., 1992, Ground penetrating radar survey design: Sensors and Software Inc., 26 p.

Balch, A.H., Lee, M.W., Miller, J.J., and Ryder, R.T., 1982, The use of vertical seismic profiles in seismic investigations of the earth: Geophysics, **47**(6), 906-918.

Beggs, G. and Garriot, J.C., Shotgun surface source: Society of Exploration Geophysicists - 49th Annual Meeting; Expanded Abstracts, S-36.

Brabham, P.J., and Goulty, N.R., 1988, Seismic refraction profiling of rockhead in the Coal Measures of northern England: Quarterly Journal of Engineering Geology, **21**, 201-206.

Cassell, B., 1984, Vertical seismic profiles - an introduction: First Break, **2**(11) 9-19.

Chen, S.T., Zimmerman, L.J., and Tugnait, J.K., Subsurface imaging using reversed vertical seismic profiling and crosshole tomography methods: Geophysics, **55**(11), 1478-1487.

Daniels, J.J., 1989, Fundamentals of ground penetrating radar: Proceedings of the Symposium on the Application of Geophysics to Engineering and Environmental Problems, 62-142.

Davis, J.L., and Annan, A.P., 1989, Ground-penetrating radar for high-resolution mapping of soil and rock stratigraphy: Geophysical Prospecting, **37**, 531-551.

Dobecki, T.L., and Romig, P.R., 1985, Geotechnical and groundwater geophysics: Geophysics, **50** (12), 2621-2636.

Fertig, J., and Krajewski, P., 1989, Acquisition and processing of pure and converted shear waves generated by compressional wave sources: Surveys in Geophysics, **10**(2-4), 103-132.

Hagedoorn, J.G., 1959, The plus-minus method of interpreting seismic refraction sections: Geophysical Prospecting, **7**, 158-182.

Hasbrouk, W.P., 1991, Four shallow-depth, shear-wave feasibility studies: Geophysics, **56**(11), 1875-1885.

Helbig, K., 1986, Shear-waves - what they are and how they can be used, *in* Danbom, S.H., and Domenico, S.N. Eds., Shear-wave exploration: Geophysical Development Series, Volume 1, Society of Exploration Geophysicists, 19-36.

Kalantzis, F., Stevens, K.M., Kanasewich, E.R., and Lodha, G.S., 1994, Depth migration of ground-penetrating radar data: CSEG & CSPG Joint National Convention, Expanded Abstracts, 251-252.

Kommedal, J.K., and Tjøstheim, B.A., 1989, A study of different methods of wavefield separation for application to VSP data: Geophysical Prospecting, **37**, 117-142.

Lankston, R.W., and Lankston, M.M., 1986, Obtaining multilayer reciprocal times through phantoming: Geophysics, **51**, 45-49.

_____, 1990, High-resolution refraction seismic data acquisition and interpretation, *in* Ward, S.H. Ed., Geotechnical and Environmental Geophysics: Volume I Review and Tutorial, Society of Exploration Geophysicists, 45-73.

Lawton, D.C., 1990, A 9-component refraction seismic experiment: Canadian Journal of Exploration Geophysics, **26** (1&2), 7-16.

McNeill, J.D., 1980*a*, Electrical conductivity of soil and rocks: Technical Note TN-5, Geonics Limited.

_____, 1980*b*, Electromagnetic terrain conductivity measurement at low induction numbers: Technical Note TN-6, Geonics Limited.

_____, 1990, Use of electromagnetic methods for groundwater studies, *in* Ward, S.H. Ed., Geotechnical and Environmental Geophysics: Volume I Review and Tutorial, Society of Exploration Geophysicists, 191-218.

Moran, S.R., 1987, Surficial geology of the Calgary urban area, Alberta Research Council, Bulletin 53.

Osborn, G.A., Thomas, R., McCoy, W.D., Miller, B., and Smith, A., 1991, Significance of a molluscan fauna to the physiographic history of the Calgary area, Alberta: Canadian Journal of Earth Science, **28** 1948-1955.

Palmer, D., 1980, The generalized reciprocal method of seismic refraction interpretation: Society of Exploration Geophysicists.

_____, 1981, An introduction to the generalized reciprocal method of seismic refraction interpretation: Geophysics, **46**(11), 1508-1518.

Smith, W.H.F., and Wessel, P., 1990, Gridding with continuous curvature splines in tension: Geophysics, **55**(3), 293-305.

Stewart, R.R., 1994, The present and promise of P-S seismic exploration: CREWES Research Report, **6**, 1.1-1.7.

Stümpel, H., Kähler, S., Meissner, R., and Milkereit, B., 1984, The use of seismic shear waves and compressional waves for lithological problems of shallow sediments: Geophysical Prospecting, **32**, 662-675.

Telford, W.M., Geldart, L.P., Sheriff, R.E., and Keys, D.A., 1976, Applied geophysics: Cambridge University Press.

Ward, S.H., 1990, Resistivity and induced polarization methods, *in* Ward, S.H. Ed., Geotechnical and Environmental Geophysics: Volume I Review and Tutorial, Society of Exploration Geophysicists, 147-189.

Wiest, B., and Edelmann, H.A.K., 1984, Static corrections for shear wave sections: Geophysical Prospecting, **32**, 1091-1102.